

1 Reconstructing hydroclimate changes of past 2,500 years 2 using speleothems from Pyrenean caves (NE Spain)

3 Miguel Bartolomé^{1,2,3*}, Ana Moreno^{4*}, Carlos Sancho^{5†}, Isabel Cacho⁶, Heather Stoll³,
4 Negar Haghpor^{3,7}, Ánchel Belmonte⁸, Christoph Spötl⁹, John Hellstrom¹⁰, R. Lawrence
5 Edwards¹¹ and Hai Cheng^{12,13,14}

6 ¹ Departamento de Geología. Museo Nacional de Ciencias Naturales (CSIC). C. de José Gutiérrez
7 Abascal, 2, 28006 Madrid, Spain.

8 ² Swiss Institute for Speleology and Karst Studies (SISKA), Rue de la Serre 68 2300 La Chaux-de-Fonds,
9 Switzerland.

10 ³ Geological Institute, NO G59, Department of Earth Sciences, Sonneggstrasse 5, ETH, 8092 Zurich,
11 Switzerland.

12 ⁴ Department of Geoenvironmental Processes and Global Change, Pyrenean Institute of Ecology (IPE-
13 CSIC), Avda. Montañana 1005, 50059 Zaragoza, Spain.

14 ^{5†} Earth Sciences Department, University of Zaragoza, C/Pedro Cerbuna 12, 50009 Zaragoza, Spain.
15 Deceased.

16 ⁶ CRG Geociències Marines, Dept. Dinàmica de la Terra i de l'Oceà, Universitat de Barcelona, 08028
17 Barcelona, Spain

18 ⁷ Laboratory for Ion Beam Physics, Department of Physics, ETH Zurich, Switzerland

19 ⁸ Sobrarbe-Pirineos UNESCO Global Geopark. Boltaña. Spain.

20 ⁹ Institute of Geology, University of Innsbruck, 6020, Innsbruck, Austria

21 ¹⁰ School of Earth Sciences, The University of Melbourne, VIC 3010, Australia

22 ¹¹ Department of Earth and Environmental Sciences, University of Minnesota, Minneapolis, MN, 55455,
23 USA

24 ¹² Institute of Global Environmental Change, Xi'an Jiaotong University, Xi'an, 710049, China.

25 ¹³ State Key Laboratory of Loess and Quaternary Geology, Institute of Earth Environment, 11 Chinese
26 Academy of Sciences, Xi'an, 710061, China.

27 ¹⁴ Key Laboratory of Karst Dynamics, MLR, Institute of Karst Geology, CAGS, Guilin, 541004, China.

28
29 * Both authors have contributed equally to this manuscript

30 *Corresponding author:* Ana Moreno (amoreno@ipe.csic.es)

31
32 **Abstract.** Reconstructing of past hydroclimates at regional scales during the Common Era (CE) is
33 necessary to place the current warming in the context of natural climate variability. Here we present a
34 composite record of oxygen isotope variations during last 2500 years based on eight stalagmites from four
35 caves in the central Pyrenees (NE Spain) dominated by temperature variations, with precipitation playing
36 a minor role. The dataset is compared with other Iberian reconstructions that show a high degree of internal
37 coherence with respect to variability at the centennial scale. The Roman Period (RP) (especially 0-200 CE),
38 the Medieval Climate Anomaly (MCA), and part of the Little Ice Age (LIA) represent the warmest periods,
39 while the coldest decades occurred during the Dark Ages (DA) and most of the LIA intervals (e.g., 520-
40 550 CE and 1800-1850 CE). Importantly, the LIA cooling or the MCA warming were not continuous or
41 uniform and exhibited high decadal variability. The Industrial Era (IE) shows an overall warming trend
42 although with marked cycles and partial stabilization during the last two decades (1990-2010). The strong
43 coherence between the speleothem data, European temperature reconstructions and global tree-ring data
44 informs about the regional representativeness of this new record as Pyrenean past climate variations. Solar
45 variability, likely through its impact on the North Atlantic Oscillation, and major volcanic eruptions appear
46 to be the two main drivers of climate in southwestern Europe during the past 2.5 millennia.

47 **Keywords.** Iberian Peninsula, Central Pyrenees, late Holocene, stalagmite, temperature reconstruction

48 1. Introduction

49 Global surface temperatures in the first two decades of the 21st century (2001–2020) were 0.84 to 1.10 °C
50 warmer than 1850–1900 CE (IPCC, 2021). There is strong evidence that anthropogenic global warming is
51 unprecedented in terms of absolute temperatures and spatial consistency over the past 2000 yr (Ahmed et
52 al., 2013; Konecky et al., 2020). On the contrary, pre-industrial temperatures were less spatially coherent,
53 and further work is needed to explain the regional expression of climate change (Mann, 2021; Neukom et
54 al., 2019). Obtaining new and high-quality records in terms of resolution, dating and regional
55 representativeness is thus critical for characterizing natural climate variability on decadal to centennial
56 scales (PAGES2k Consortium et al., 2017).

57 High mountains are particularly sensitive regions to climate change and among them the Pyrenees occupy
58 a crucial frontier position in southern Europe, influenced by both Mediterranean and Atlantic climates. In
59 the Pyrenees, the temperature has increased by more than 1.5°C since 1882, as shown by the longest time
60 series from the Pic du Midi observatory (Bücher and Dessens, 1991; Dessens and Bücher, 1995). Recent
61 studies confirm this warming trend, showing an increase of 0.1 °C per decade during the last century in
62 Central Pyrenees (Pérez-Zanón et al., 2017), or even 0.28°C per decade if only the 1959-2015 period is
63 considered (Observatorio Pirenaico de Cambio Global, 2018). Long-term snow depth observations (starting
64 in 1955) show a statistically significant decline, especially at elevations above 2000 m a.s.l. (López-Moreno
65 et al., 2020). This fact, together with the increase in temperature, has caused the glaciated area in the
66 Pyrenees to decrease by 21.9% in the last decade (Vidaller et al., 2021), changing from 2060 ha during the
67 LIA to 242 ha in 2016 (Rico et al., 2017). Recent studies on one of the emblematic glaciers in the Pyrenees,
68 the Monte Perdido glacier, show that the current ice retreat is unprecedented in the last 2000 years, as this
69 glacier survived previous warm periods such as the MCA and the RP (Moreno et al., 2021b).

70 The study of sediment records from lakes in the Pyrenees, where considerable variations in water level,
71 water chemistry, and biological processes have occurred due to changes in effective moisture and
72 temperature, is an excellent approach to reconstruct past climate variability (González-Sampérez et al.,
73 2017). Recently, a comprehensive study in six high altitude Pyrenean lakes indicates unprecedented
74 changes in the lithogenic and organic carbon fluxes since 1950 CE, suggesting an increase in algal
75 productivity likely favoured by warmer temperatures and higher nutrient deposition associated to the Great
76 Acceleration (Vicente de Vera García et al., 2023), a period when human-driven global, social,
77 technological, and environmental changes intensifying dramatically (Steffen et al., 2015). Marine records
78 off the Iberian coast show a clear long-term cooling trend, from 0 CE to the beginning of the 20th century,
79 probably reflecting the decline in Northern Hemisphere summer insolation that began after the Holocene
80 optimum (Abrantes et al., 2017). Unfortunately, it is not possible to record decadal temperature changes
81 from the studied proxies of these lake or marine records, so other archives allowing higher chronological
82 robustness and larger resolution are required.

83 The Central Pyrenees are largely composed of limestones and host numerous caves, some of which are rich
84 in speleothems, thus making it possible to reconstruct the past climate by studying stalagmites from
85 different caves. Unfortunately, despite the high potential of stalagmite with annually to sub-annual
86 resolution in the CE, it is extremely difficult to obtain high-resolution and well-replicated records. In most
87 cases, the CE period spans only a few centimetres, limiting the number of samples drilled for high-precision
88 U-Th dating (PAGES Hydro2k Consortium, 2017). In addition to this chronological challenge, the
89 interpretation of oxygen isotopes of speleothems ($\delta^{18}\text{O}_c$) from southern Europe is also complex (Moreno et
90 al., 2021a). Recent studies of Pyrenean stalagmites covering the last deglaciation indicate the important
91 role of changes in annual temperature in the variability of $\delta^{18}\text{O}_c$ (Bartolomé et al., 2015a; Bernal-Wormull
92 et al., 2021). However, correct interpretation of $\delta^{18}\text{O}_c$ proxies requires a sound understanding of the
93 influence of climate variables on carbonate deposition in caves through monitoring (e.g. Pérez-Mejías et
94 al., 2018) and calibration to the instrumental period (Mangini et al., 2005; Tadros et al., 2022).

95 In this study, we provide high-resolution $\delta^{18}\text{O}_c$ data for eight stalagmites from four different caves in the
96 Central Pyrenees, allowing us to construct a stacked curve of climate variability for the last 2500 years with

97 potential regional representativeness. These eight stalagmites allow climate changes during the CE to be
98 studied in reasonably robust chronological framework. Monitoring and calibration of $\delta^{18}\text{O}_c$ with
99 instrumental data for the two youngest stalagmites suggests that the $\delta^{18}\text{O}_c$ variability primarily reflects
100 annual temperatures, while precipitation played a role during certain periods. This new record represents
101 an excellent opportunity to characterize natural temperature changes in this region on decadal to centennial
102 scales for the last 2500 years and compare them with other approaches to examine their regional
103 representativeness.

104 **2. Study sites**

105 **2.1. Geological setting, climate and vegetation**

106 This study of speleothems is located in the central sector of the Pyrenees, in northeastern Iberia (Fig. 1a,b).
107 All caves are located in the Sobrarbe Geopark, close to or at the borders of the Ordesa and Monte Perdido
108 National Park, formed in Mesozoic and Cenozoic limestones and at different altitudes (Fig. 1c). This area
109 has a steep topography due to the high altitudinal gradient and constitutes the largest limestone massif in
110 Europe (with 22 peaks above 3000 m a.s.l.).

111 The climate is Mediterranean according to the Köppen classification. However, the high relief influences
112 the climate of this high-altitude area which is accurately described as humid sub-Mediterranean because of
113 higher rainfall than the typically Mediterranean climate, particularly for the caves above 1000 m a.s.l. where
114 annual precipitation is above 1000-1200mm and falls mostly as snow. In lower altitude caves (e.g. Seso
115 Cave) mean annual precipitation is 900 mm, concentrated in spring and fall. Mean air temperatures range
116 from 0.5 to 15°C, depending on the altitude.

117 Around the caves, in the valleys, there are mid-mountain forests dominated by *Pinus sylvestris* and *Quercus*
118 *ilex*, as well as shrublands, whereas the highlands are characterized by exposed rock with sparse vegetation
119 such as meadows.

120 **2.2. Cave locations**

121 Seso cave (42°27'23.08"N; 0°02'23.18"E, 794 m a.s.l.) is formed in the eastern flank of the Boltaña
122 Anticline, close to Boltaña village. The cave developed in insoluble marly strata between limestone beds
123 of Eocene age. The cave system consists of two longitudinal shallow galleries (2-3m of limestone thickness
124 over the cave) controlled by the bedding and the main set of joints. Formation of this shallow cave involved
125 the mechanical removal of large amounts of marl under vadose conditions which took place about 60-40
126 ka BP (Bartolomé et al., 2015b). Subsequently, calcite speleothems formed which became more abundant
127 during the Holocene. Average annual temperature inside Seso cave is ~11.8°C.

128 Las Gloces cave (42°35'40" N, 0°1'41"W, 1243 m a.s.l.) is located on the border of the Ordesa National
129 Park, next to Fanlo village. The cave formed in limestones of Early Eocene age. The limestone's thickness
130 above the cave is ~20-30 m. Two galleries form the cave. The upper one preserves phreatic features and
131 hosts the majority of speleothems located in a small room, while vadose morphologies characterize the
132 lower gallery. Average annual temperature where the stalagmites were taken is ~ 9.8 °C

133 B-1 cave (42°36'0.2"N; 0°7'46"E; 1090 m a.s.l.) is the lower entrance of the Las Fuentes de Escuaín
134 karstic system, and acts as the collector of all water drained by the system. This system comprises more
135 than 40 km of galleries and shows a vertical extension of -1150 m. It drains an area of ~15 km² and
136 developed mostly in Eocene limestones. Since a river runs through the cave, several detrital sequences
137 appear, as well as speleothems, affected by floods. The cave is then well ventilated and shows annual
138 temperature variations in response to the seasonal ventilation changes and seasonal flooding. The studied
139 sample was obtained in a fossil gallery, not currently influenced by flooding and with an average annual
140 temperature of ~9.5°C.

141 Pot au Feu cave (42°31.48' N; 0°14.26' W; 996 m a.s.l.) is located in the Irués river valley in the Cotiella
142 massif. The host rock is an Upper Cretaceous limestone. Hydrogeologically, the cave belongs to the high
143 mountain unconfined karst Cotiella-Turbón aquifer but located in a non-active level. The cave comprises
144 horizontal galleries and small rooms connected by shafts formed by phreatic circulation. Some rooms are
145 well-decorated by large speleothems. The limestone thickness over the gallery where the stalagmite was
146 collected is approximately 800 m.

147 **2.3. Cave climate**

148 Understanding the modern microclimatic and hydrological conditions of caves is important for a sound
149 interpretation of speleothem proxy data (Genty et al., 2014; Lachniet, 2009; Moreno et al., 2014).
150 Particularly, the transfer of the stable isotopic signal from the rainfall to the dripwater and, eventually, to
151 the studied stalagmite is influenced by different processes in the atmosphere, soil and epikarst. Our
152 preliminary results for the Pyrenees show a seasonal pattern of precipitation isotopes consistent with the
153 annual temperature cycle (Moreno et al., 2021b). These data also suggest an interannual temperature– $\delta^{18}\text{O}$
154 relationship of 0.47‰/°C (Giménez et al., 2021) that is only partially compensated by the -0.18 ‰/°C due
155 to the water-calcite isotope fractionation (Tremaine et al., 2011) thus allowing to use $\delta^{18}\text{O}$ in speleothems
156 as a temperature indicator in this region (see also Bartolomé et al., 2015a; Bernal-Wormull et al., 2021).

157 From the four studied caves, the best monitored one is Seso cave where a detailed monitoring survey was
158 conducted including analyses of $\delta^{18}\text{O}$ variability in rainfall, soil water, dripwater and farmed calcite
159 (Bartolomé, 2016). Seso cave developed under just few metres of rock, while the other caves are much
160 deeper, allowing a faster response to rainfall variability in Seso dripwaters and speleothems. Monitoring
161 carried out in Seso cave indicates a relationship between temperature and $\delta^{18}\text{O}$ of rainfall observed at
162 seasonal scale while rainfall isotopic composition is slightly modulated by the precipitation (Bartolomé et
163 al., 2015a).

164 **3. Methods**

165 **3.1. Speleothem samples**

166 This study is based on eight stalagmites from four different caves in Central Pyrenees (Fig. 1c, Table 1).
167 The specimens were cut parallel to the growth axis and the central segment was sampled for U-Th dating,
168 stable isotopes ($\delta^{18}\text{O}$ and $\delta^{13}\text{C}$) and Mg/Ca. Furthermore, the ^{14}C -activity of multiple samples from the top
169 of stalagmites MIC and XEV (both from Seso cave and underneath active drips) was determined in order
170 to detect the atmospheric bomb peak induced by the nuclear tests in 1945-1963.

171 Four small stalagmites were obtained from Seso cave, all showing fine laminations consisting of pairs of
172 dark-compact and light-porous laminae, but difficult to count due to their irregular pattern. The four Seso
173 stalagmites show medium to high porosity in some intervals, usually more frequent towards the top. MIC
174 (8.5 cm long) and XEV (26 cm long, composed of two stacked stalagmites – Appendix Fig. A1.a) were
175 sampled from base to top. In stalagmites CHA (8.5 cm long) and in CLA (10.5 cm long), the uppermost
176 interval was discarded due to the poor chronological control and associated to a possible hiatus above a
177 macroscopic discontinuity (Fig. A1.a).

178 Stalagmites ISA (13.5 cm long, with a visual hiatus at 7 cm above the base) and LUC (23.3 cm long, also
179 with a hiatus at 12.5 cm above the base) were sampled in Las Gloces cave (Fig. A1.b). Both are candle-
180 shaped with a slight tilt in the growth axis above their respective hiatus. One stalagmite, TAR, was obtained
181 from B1 cave which is an overgrowth over an older stalagmite composed of 7.5 cm of white carbonate that
182 is slightly laminated towards the top (Fig. A1.c). Finally, a 80 cm-long stalagmite (JAR) was obtained from
183 Pot au Feu cave. It is candle-shaped, laminated and lacks macroscopic hiatuses (Fig. A1.d).

184 **3.2. Stable isotope and Mg/Ca analyses**

185 Samples for stable isotopic ($\delta^{18}\text{O}$ and $\delta^{13}\text{C}$) analyses were microdrilled at 1-mm resolution along the growth
186 axis of seven of the eight speleothems (JAR from Pot au Feu was sampled every 5 mm) using a 0.5 mm
187 tungsten carbide dental bur. The first batch of the isotopic analyses was analysed at the University of
188 Barcelona (Scientific-Technical Services), Spain, using a Finnigan-MAT 252 mass spectrometer, linked to
189 a Kiel Carbonate Device III, with a reproducibility of 0.02‰ for $\delta^{13}\text{C}$ and 0.06‰ for $\delta^{18}\text{O}$. Calibration to
190 Vienna Pee Dee Belemnite (VPDB) was carried out by means of the NBS-19 standard. A second batch was
191 analysed at the University of Innsbruck using a ThermoFisher Delta V Plus isotope ratio mass spectrometer
192 coupled to a ThermoFisher GasBench II. Calibration of the instrument was accomplished using
193 international reference materials and the results are also reported relative to VPDB. Long-term precision
194 on the 1-sigma level is 0.06‰ and 0.08‰ for $\delta^{13}\text{C}$ and $\delta^{18}\text{O}$, respectively (Spötl, 2011).

195 The elemental chemical composition was analysed in the eight stalagmites (every 1 mm in Las Gloces,
196 Seso and B1 stalagmites and every 5 mm in JAR from Pot au Feu cave) using matrix-matched standards on
197 an inductively coupled plasma-atomic emission spectrometer (Thermo ICAP DUO 6300 at the Pyrenean
198 Institute of Ecology) following the procedure described in Moreno et al. (2010). Reported ratios are from
199 measurement of Ca (315.8 nm) and Mg (279.5 nm), all in radial mode.

200 **3.3. U-Th dating and ^{14}C bomb peak**

201 A total of 55 samples were prepared for U-Th dating, according to the U and Th chemical procedures
202 described in Edwards et al. (1987). Sample portions characterized by high porosity and voids were avoided
203 to minimize the effect of open system behaviour and possible age inversions. From those 55 samples, 45
204 were measured at the University of Minnesota (USA) and at the Xian' Jiaotong University (China) while
205 10 samples were analysed at the University of Melbourne (Australia) (samples of JAR) using the
206 methodology described in Hellstrom (2006). In the three laboratories, measurements were performed using
207 a MC-ICP-MS (Thermo-Finnigan Neptune or Nu Instruments) following previously described methods
208 (Cheng et al., 2013).

209 Due to the low U content (Table 2), the U-Th ages are not precise enough to obtain an accurate chronology
210 for the recent speleothem growth (see large errors in top samples in Fig. A1). Therefore, the ^{14}C “bomb
211 peak” method was applied to the MIC and XEV stalagmites that were actively growing in Seso cave at the
212 time of collection (2010 and 2013, respectively), confirmed by U/Th ages, albeit of low precision. We
213 drilled 10 and 8 subsamples for MIC and XEV, respectively (Fig. 2a and b), and ^{14}C activities were
214 measured using a novel online sampling and analysis method combining laser ablation with accelerator
215 mass spectrometry (LA-AMS) at the ETH Zurich (Welte et al., 2016). LA-AMS allows to produce spatially
216 resolved ^{14}C profiles of carbonate minerals with a precision of 1% for modern samples. The background
217 measured on ^{14}C -free marble ($F^{14}\text{C} = 0.011 \pm 0.002$) is low and reference carbonate material is well
218 reproduced. This method relies on the exploitation of the global anthropogenic increase in atmospheric ^{14}C
219 resulting from nuclear testing predominately in the 1950s and 1960s CE as a chronological marker in the
220 mid to late 20th Century (e.g., Genty et al., 1998; Hua et al., 2012). Atmospheric ^{14}C concentrations began
221 to rise in 1955 CE, peaking in the Northern Hemisphere (NH) in 1963 CE (Reimer, 2004). Because 80 to
222 90% of the carbon found in most speleothems comes from soil CO_2 , this being linked to atmosphere CO_2 ,
223 it is likely that speleothem ^{14}C activity is close to the atmospheric ^{14}C activity or at least to the soil activity
224 (Markowska et al., 2019). Thus, the point where the ^{14}C concentration begins to rise, the highest
225 concentration point, and the date when the speleothem was removed from the cave (if actively dripping)
226 were used as chronological anchor points (Fig. 2a and b).

227 **3.4. Age model**

228 Age models were produced using StalAge software (Scholz and Hoffmann, 2011) for the eight speleothems
229 (Fig. A1) using the U-Th dates presented in Table 2. In the ISA stalagmite, one date was discarded due to
230 the large error (indicated in red in Table 2). During several intervals, two or more stalagmites grew
231 contemporaneously, allowing to test the reproducibility of the proxy records. We made the a priori
232 assumption that the $\delta^{18}\text{O}$ data of the selected stalagmites record a common rainfall and temperature signal,

233 given that these caves were only 20 km apart (Fig.1c). Then, the records are combined with *Iscam*
234 (Fohlmeister, 2012), a method that correlates dated proxy signals from several stalagmites, determines the
235 most probable age-depth model, and calculates the age uncertainty for the combined record.

236 In order to minimize the effect of different absolute isotopic values and ranges of individual stalagmite data
237 series, we detrended and normalized the $\delta^{18}\text{O}$ series using *Iscam*. Doing so, the interpretation of absolute
238 values will be precluded. Regarding the other parameters that can be changed in *Iscam*, we used point-wise
239 linear interpolation, 1000 Monte Carlo simulations and the smoothing window was fixed at 10 years. The
240 stalagmites were included in the *Iscam* composite record from the oldest to the youngest one as was the
241 order that provided the highest correlation coefficients: JAR- LUC – ISA -TAR – CHA – CLA -XEV and
242 MIC. The ISA sample was treated as two parts (ISA top and ISA base) to account for the hiatus, while LUC
243 was regarded as only one as *StalAge* does not suggest a hiatus in this stalagmite (Fig. A1.b). For the two
244 stalagmites that were active when collected, MIC and XEV, we also produced a composite record for the
245 last 200 years using *Iscam* (Fig. 2c).

246 In order to explore correlations among stalagmites from the same caves, we repeated the procedure to obtain
247 a composite record for the four stalagmites from Seso cave (CHA, CLA, XEV and MIC) (Fig. A2) and the
248 two from Las Gloces cave (ISA and LUC) (Fig. A3). In those two cases, we did not detrend or normalize
249 the individual records since they belong to the same cave and show the same range of $\delta^{18}\text{O}$ values. These
250 four records (composite records from Las Gloces and Seso caves, and individual stalagmites from Pot au
251 Feu and B1 caves) are show in Fig. 3 and compared to the final composite record. The composite $\delta^{18}\text{O}$
252 record is used in this article as a proxy record for the Central Pyrenees climate of last 2500 years. We have
253 used approximate onset and end of five time subperiods, following previous literature (eg. Sánchez-López
254 et al., 2016): the end of the RP at 450 CE; DA (450-850 CE), MCA (850-1250 CE), LIA (1250-1950 CE)
255 and IE (since 1850 CE).

256 **3.5. Statistical analyses**

257 Statistical analyses were carried out using PAST software (Hammer et al., 2001). The $\delta^{18}\text{O}$ series and the
258 instrumental climatic series were first resampled (linear interpolation) to obtain the same regular spacing
259 (annual). Then, correlation was computed using Spearman's rank correlation analysis, a nonparametric
260 measure as an alternative to Pearson correlation analysis. This analysis was preferred to account for
261 nonlinear relationships, with r indicating the correlation coefficient and p -value, the probability value of
262 that correlation. The Bonferroni test was applied to prevent data from spuriously appearing as statistically
263 significant by making an adjustment during comparison testing (PAST software; Hammer et al, 2001).

264

265 **4. Results**

266 **4.1. Age models and composite record**

267 **4.1.1. Detection of the bomb peak and composite record of the last 200 years**

268 Stalagmites MIC and XEV from Seso cave were actively dripping when removed from the cave (in 2010
269 and 2013, respectively). Calcite deposited on glass plates placed below the two dripping points and
270 collected seasonally until 2021 demonstrates that the drip water is supersaturated with respect to calcite and
271 suggests that the top layer of both stalagmites was formed during the respective collection year (Fig. 2).
272 Therefore, these two stalagmites were analysed for their ^{14}C activity to identify the “bomb peak” and
273 improve the age model.

274 A strong increase in the ^{14}C activity is registered in the MIC and XEV stalagmites at 16 mm and 40 mm
275 depth from top (dft), respectively (Fig. 2a and b) with a rise in the fraction modern $F^{14}\text{C}$, interpreted as the
276 start of the mid-20th century atmospheric bomb peak. This allows defining the year 1955 CE, within $\pm 2\text{yr}$
277 uncertainties, at 16 mm dft in MIC and 40 mm dft in XEV (Fig. 2). All radiocarbon bomb peaks published

278 from speleothems show that the response of speleothem ^{14}C activity to the increase in atmospheric
279 radiocarbon activity occurred nearly simultaneously. However, whether the ^{14}C activity peak in a
280 speleothem can be assigned to the year 1963 CE depends on the soil properties and the thickness of the
281 rock above the cave, as well as the delay in the transfer of the atmospheric ^{14}C signal to the speleothem
282 (Fohlmeister et al., 2011; Hua et al., 2017). In the case of Seso cave, which is just 2-3 m below the surface
283 and the soils are patchy and thin (Bartolomé, 2016), the transfer of the ^{14}C signal was likely fast. We
284 therefore place the year 1963 CE, within $\pm 2\text{yr}$ uncertainties, at 11 mm dft in MIC and at 25 mm dft in XEV
285 (Fig. 2a and b).

286 Since the two stalagmites MIC and XEV are the only ones in this study whose records extend to modern
287 times, we compare them with the instrumental record in order to improve the interpretation of the stable
288 isotope data. Thus, MIC and XEV $\delta^{18}\text{O}$ data were first combined using *Iscam* (Fig. 2c). Using the
289 parameters indicated in Methods (section 3.3), but without normalizing the records (both stalagmites belong
290 to the same cave and show the same range of $\delta^{18}\text{O}$ values) the correlation of stalagmites MIC and XEV
291 provided by *Iscam* software (r is 0.81 (95% significance). This composite $\delta^{18}\text{O}$ record covers the last 200
292 years and has an amplitude of 0.9 ‰. The main feature (Fig. 2c) is a trend towards less negative values
293 (indicated by a polynomial line in Fig. 2c).

294 **4.1.2. StalAge models and Iscam stack**

295 Age models obtained by StalAge for individual stalagmites indicate that the growth rate was quite stable,
296 except of ISA and LUC, both from Las Gloces cave, where the growth rate changed after hiatuses (Fig.
297 A1.B). The temporal resolution of the stable isotope data allows to explore changes occurring on a decadal
298 scale (Table 1).

299 Using the parameters for constructing a composite record using *Iscam* (see Methods), correlation (r) value
300 (95% significance) of stalagmite JAR and LUC is 0.48, 0.67 between ISA_base and the combined stack of
301 JAR-LUC, 0.65 between ISA_top and the previous stack, 0.74 between TAR and the previous stack, 0.79
302 between CHA and the previous stack, 0.95 between CLA and the previous stack, 0.71 between XEV and
303 the previous stack and finally, 0.53 between MIC and the previous stack. These values demonstrate a
304 statistically significant correlation among the individual stalagmites and a higher correlation than between
305 the original time series. The composite $\delta^{18}\text{O}$ record was compared to the composite records from Seso (Fig.
306 A3) and Las Gloces (Fig. A4) caves and the two individual stalagmites from the other two caves (Fig. 3).
307 This comparison shows that many of the main features of the original records are also well recorded in the
308 composite (Fig. 3). One example is the interval 530-550 CE during the Dark Ages characterized by
309 relatively low $\delta^{18}\text{O}$ values in Las Gloces and Pot au Feu cave records (black arrows in Fig. 3), or the interval
310 at the end of the LIA (1675-1750 CE) with less negative $\delta^{18}\text{O}$ values in Seso, B1 and Las Gloces cave
311 records (this interval is recorded in five stalagmites: CHA, XEV, TAR, LUC and ISA, Figs. A1).

312 **4.2. Individual isotopic and Mg/Ca profiles and composite $\delta^{18}\text{O}$ record**

313 The isotopic ($\delta^{18}\text{O}$ and $\delta^{13}\text{C}$) and Mg/Ca profiles are shown for the eight stalagmites, using their StalAge
314 models (Fig. A1) for the four caves studied (Seso, Las Gloces, B1 and Pot au Feu). In general, $\delta^{18}\text{O}$ and
315 $\delta^{13}\text{C}$ are not well correlated ($r \sim -0.3-0.4$; p -values indicating no significant correlation) with the exception
316 of TAR ($r > 0.8$) and CHA ($r = 0.5$). Generally, $\delta^{13}\text{C}$ is better correlated with Mg/Ca pointing to a
317 hydrological link of these proxies, via changes in prior calcite precipitation (PCP) associated with the longer
318 residence time of the water in the soil and epikarst during dry periods (Genty et al., 2006; Moreno et al.,
319 2010). A similar interpretation was suggested for other Holocene records from northeastern Spanish caves,
320 such as speleothems from Molinos-Ejúlve caves in the Iberian Range (Moreno et al., 2017) and records
321 covering the last deglaciation in the Pyrenees (Bartolomé et al., 2015a). However, $\delta^{13}\text{C}$ and Mg/Ca are
322 highly variable in absolute values and patterns among caves, and further studies are required to better
323 constrain the climate-proxy transfer functions for two parameters. Therefore, we base our paleoclimate
324 interpretations on the oxygen isotopes which are known to show a more robust response to regional climate
325 change.

326 The composite $\delta^{18}\text{O}$ record for the Central Pyrenees of the last 2500 years is shown in Fig. 3. The highest
327 $\delta^{18}\text{O}$ values of last 2500 years were reached during the RP (50 BCE-250 CE). The MCA is characterized
328 by two intervals of relatively high values (900-950 CE and 1150-1250 CE) and also the LIA shows a one
329 such interval (1675-1750 CE). In contrast, the Dark Ages are characterised by consistently low values. In
330 fact, the most negative interval of last 2500 years is reached at \sim 520 CE, a well-known cold episode related
331 to volcanic eruptions (see section 5.2). A long interval with low $\delta^{18}\text{O}$ values corresponds to the onset of the
332 LIA (1250-1500 CE, with two very negative excursions) as well as the end of the LIA (1750-1850 CE).
333 The most remarkable feature of the MCA and LIA is the large centennial-scale variability. In fact, the LIA
334 has a clear tripartite pattern, with two intervals of low values at the onset and end and less negative values
335 in between. In contrast, the MCA pattern, although also tripartite, it is characterized by two intervals of less
336 negative values at the onset and end, and a short period of low values in between. An interval with high
337 $\delta^{18}\text{O}$ values is observed since 1950 CE (Fig. 3).

338

339 5. Discussion

340 5.1. Interpretation of $\delta^{18}\text{O}$ data

341 Under equilibrium conditions, the $\delta^{18}\text{O}$ value of speleothem carbonate is related to just two variables: the
342 $\delta^{18}\text{O}$ value of the drip water, and the cave temperature through its control on equilibrium isotope
343 fractionation between water and calcite (Lachniet, 2009). Over the CE, air temperature in a given cave
344 likely changed very little ($< 1\text{ }^\circ\text{C}$ corresponding to \sim 0.18‰ in stalagmite $\delta^{18}\text{O}$, following Tremaine et al.,
345 2011) (PAGES Hydro2k Consortium, 2017) such that the observed $\delta^{18}\text{O}$ variations in these Pyrenean
346 speleothems of more than 1‰ are governed primarily by the $\delta^{18}\text{O}$ variability of the drip water.

347 For a constant sea-surface $\delta^{18}\text{O}_{\text{sw}}$ value, as it is expected for this time period, event-scale monitoring of the
348 isotopic composition of oxygen in the rainwater ($\delta^{18}\text{O}_{\text{r}}$) in different areas of the Iberian Peninsula constrains
349 some of the drivers of rainfall isotopic fractionation (Moreno et al., 2021b). Recent rainfall monitoring
350 surveys in the Central Pyrenees indicate that the values of $\delta^{18}\text{O}_{\text{r}}$ show an interannual dependence on
351 temperature equivalent to 0.47–0.52‰/°C, depending on the site (Giménez et al., 2021; Moreno et al.,
352 2021a). This dependence is only partially offset by the empirical value of isotope fractionation during
353 calcite precipitation ($-0.18\text{‰}/^\circ\text{C}$; Tremaine et al., 2011) thus allowing to consider temperature as one
354 important factor driving $\delta^{18}\text{O}$ variability. Apparently, the rainfall amount does not strongly control the
355 isotopic values at event-scale, but analysing the $\delta^{18}\text{O}_{\text{r}}$ variation through time, added to the strong
356 dependence on air temperature, it is clearly observed how the most intense rainfall events together with the
357 longest lasting rain events (several days) resulted in an isotopic lightening (Giménez et al., 2021). Thus, we
358 consider that dripwater $\delta^{18}\text{O}_{\text{dw}}$ is driving the $\delta^{18}\text{O}_{\text{c}}$ signal in the stalagmites and, very likely, air temperature
359 and precipitation amount will be modulating its variability along last 2500 years.

360 The $\delta^{18}\text{O}$ composite record, based on the combination of MIC and XEV $\delta^{18}\text{O}$ data, provides the opportunity
361 to correlate with instrumental temperature and precipitation data (Fig. A4 and A5). It is worth to note that
362 the chronological control of $\delta^{18}\text{O}$ data is robust at decadal-scale, thus limiting an annual accurate
363 correlation. In spite temperature records in the region of the studied caves are, unfortunately, scarce and
364 short (e.g., the Goriz hut station covers only the last 50 years, Fig. A4b) there are two exceptions. First, the
365 homogenized MAAT dataset since 1882 from the Pic du Midi de Bigorre meteorological station (2860 m
366 a.s.l. in the French Pyrenees) (Bücher and Dessens, 1991; Dessens and Bücher, 1995), which started in
367 1882 CE, is the currently longest one from the Pyrenees (Fig. A4c). And, second, the temperature and
368 precipitation reconstruction by Pérez-Zanón et al. (2017) based on 155 stations from the Central Pyrenees
369 starting in 1910 CE (Fig. A4d). Comparing the MIC and XEV $\delta^{18}\text{O}$ data with those temperature datasets a
370 significant correlation is found with Pic du Midi de Bigorre mean annual minima temperature ($\sigma_s = 0.32$; p-
371 value < 0.005). Likely, the other temperature records were too short to generate a significant correlation.

372 Additionally, when comparing our $\delta^{18}\text{O}$ stack with the HadCRU5 reconstruction for the mean Northern
373 Hemisphere temperatures (Morice et al., 2021) (Fig. A4e), the correlation is higher and significant (σ_s

374 =0.49; p-value<0.005). We suspect that the length of this last series (150 years) together with a large spatial
375 scale leads to a better correlation with the speleothem composite. However, a large part of the variance
376 remains to be explained by other factors (i.e. precipitation changes in source, seasonality or amount). Using
377 these relationships as a guide and considering all the isotopic change related to temperature change, the
378 observed variation of 0.30 – 0.32 ‰ in $\delta^{18}\text{O}$ of our composite would represent a change of 1°C (Fig. A4),
379 that appears quite plausible for the studied period.

380 The influence of precipitation variability on the $\delta^{18}\text{O}$ speleothem composite is evident from 1970 to 1980
381 CE, a relatively cool interval in the Pyrenees but characterized by a sustained decrease in
382 precipitation (Pérez-Zanón et al., 2017) (Fig. A5, note reversed axis for precipitation). For this interval, the
383 relationship between the $\delta^{18}\text{O}$ composite and temperature series is reversed, as the low precipitation leads
384 to higher $\delta^{18}\text{O}$ values (as if they represented higher air temperatures). On the contrary, a rapid increase in
385 precipitation at ca. 1960 without any important change in temperature, results in a negative peak on the
386 $\delta^{18}\text{O}$ speleothem composite (Fig. A5). This shows that, in spite air temperature being an important factor
387 influencing $\delta^{18}\text{O}$ variability in speleothems from the Pyrenees, other processes such as the amount of
388 precipitation or even its source(s) may be also a significant controlling factor (Priestley et al., 2023; Treble
389 et al., 2022), especially when extreme values are reached (very dry or very wet time intervals), as was
390 indicated by rainfall studies in the Pyrenees (Giménez et al., 2021; Moreno et al., 2021a). In any case, MIC
391 and XEV $\delta^{18}\text{O}$ data are not significantly correlated with any of the precipitation data from Fig. A5.

392 Finally, it is important to note that the $\delta^{18}\text{O}$ values in the different caves varied at distinct range (Fig. 3).
393 Thus, when producing the composite record, the $\delta^{18}\text{O}$ profiles of the eight stalagmites were normalized and
394 detrended with the aim of combining different caves. With such a procedure, comparing relative
395 temperature changes coming from different time periods is not possible. Thus, for example, comparing the
396 warming magnitude of the RP with the MCA or with the IE is not feasible since data were obtained from
397 different caves and were previously normalized and detrended. Unfortunately, none of our stalagmites
398 cover continuously from a warm period, i.e. the MCA, to current conditions to compare values. Therefore,
399 the ability of current data to accurately quantify changes in temperature for last 2500 years in the Central
400 Pyrenees is limited. Normalized $\delta^{18}\text{O}$ composite record is evaluated in the context of previous local,
401 regional and global information.

402 **5.2 Climate reconstruction for the last 2500 years**

403 The Pyrenees is a region threatened by global warming, where the impact on biodiversity, elements of the
404 mountain cryosphere such as glaciers or ice caves, and water resources has been increasing in recent
405 decades (<https://www.opcc-ctp.org>). The $\delta^{18}\text{O}$ composite constructed using eight speleothems represents
406 the first climate reconstruction based on speleothems for this region covering the last 2500 years and
407 provides an excellent opportunity to reconstruct natural variability and disentangle main driving
408 mechanisms. We compare it first with other climate series from the Pyrenees and northern Iberia (section
409 5.2.1) and, then, with available speleothems from Europe and western Mediterranean to obtain a regional
410 overview (section 5.2.2). Finally, a short discussion about the potential drivers of main observed changes
411 is provided (section 5.2.3).

412 **5.2.1. The last 2500 years in the context of the Iberian Peninsula**

413 Previous climate reconstructions for the CE from the Pyrenees were mostly based on lake records (e.g.,
414 González-Sampéris et al., 2017), tree-ring data (e.g., Büntgen et al., 2017), and few data from glaciers or
415 ice caves (Moreno et al., 2021b; Oliva et al., 2018; Sancho et al., 2018; Leunda et al., 2019). Despite large
416 variability, these records reveal a clear distinction between relatively cold (DA, LIA) and warm (RP, MCA)
417 periods, which were generally characterized by high and low lake levels, respectively. The differences and
418 similarities among Pyrenean records merit a more detailed evaluation, organized by chronological periods.

419 A. The Iberian - Roman period in the Pyrenees. Considering the last 2500 years, the RP stands out as a
420 clear warm period from the speleothem composite record (Fig. 4a). In the Eastern Pyrenees, Redon Lake

421 records low winter-spring temperatures with a warming trend at the end (Pla and Catalan, 2005; Pla-Rabes
422 and Catalan, 2011), whereas the summer-autumn temperatures show a transition from cold to warm
423 (Catalan et al., 2009). Not many high-resolution Pyrenean lake records exist for this period (e.g. Corella et
424 al., 2016; Vegas-Vilarrúbia et al., 2022) and dendrochronological studies in this mountain range do not
425 cover this time period. Thus, an interesting record to compare with is the A294 ice cave in the Cotiella
426 massif (Sancho et al., 2018). This 9-m thick ice is divided into intervals of low and high snow accumulation,
427 requiring moist and cold conditions to form. The fourth (and last) stage of this ice deposit indicates a high
428 accumulation rate (Fig. 4d), thus a relatively humid and cold period, from 500 BC to 62 CE. Afterwards,
429 the record stopped reflecting the onset of a warmer and drier climate (Sancho et al., 2018) associated with
430 the RP thermal maximum (Fig 4a). Recently, not yet published observations indicate the ice deposit grew
431 during the cold/wet years associated to the DA (M. Bartolomé, personal communication). In our speleothem
432 composite, the RP is represented by Las Gloces and Pot au Feu stalagmites that show less negative values
433 (Fig. 3), which suggest rather warm, and probably dry conditions in the Central Pyrenees during the RP,
434 particularly between 0 to 200 CE (Fig. 4). This is supported by data showing retreating glaciers in the
435 Pyrenees at that time (Moreno et al., 2021b).

436 B. The Dark Ages in the Pyrenees. This period is characterized in our speleothem composite by cold-wet
437 climates starting ca. 300 CE, with two particular cold events at 500-650 CE and 750-850 CE and a warmer-
438 drier interval in between (650-750 CE) (Fig. 4a). Pyrenean lake records also point to cold and wet conditions
439 but with a high heterogeneity and low resolution, thus preventing a detailed characterization of this time
440 period (González-Sampéris et al., 2017). For example, Estanya Lake recorded a dominant dry climate
441 between 500 and 750 CE (Fig. 4c), changing to higher lake levels afterwards (Morellón et al., 2009), a
442 pattern that is quite coherent with the speleothem composite. Proxy data from Redon Lake suggest cold
443 winter-spring temperatures in the Eastern Pyrenees during the DA (Pla and Catalan, 2005, 2011).

444 C. The Medieval Climate Anomaly in the Pyrenees. The large centennial-scale temperature variability
445 recorded by the speleothem composite is particularly well expressed for the MCA and the LIA, with three
446 distinct intervals of temperature changes (yellow and blue bands in Fig. 4a), thus revealing a more complex
447 pattern as previously inferred by lower resolution records (e.g., Moreno et al., 2012; Sánchez-López et al.,
448 2016). The MCA has been interpreted as a “warm and dry” climate regime in the Southern Pyrenees
449 (Morellón et al., 2012) (Fig. 4c), characterized by low lake levels and more abundant xerophytic vegetation.
450 Our new data show, however, that a colder (maybe wetter) interval between 950 and 1050 CE separated
451 two clear warm periods before (900-950 CE) and after (1150-1250 CE; Fig. 3). This cold interval was also
452 identified in the Redon Lake record as a sudden cooling about 1000 years ago (Pla and Catalan, 2005).
453 Interestingly, this cold century was not observed by an increase in precipitation in the Montcortés lake
454 record (Fig. 4b).

455 D. The Little Ice Age in the Pyrenees. The LIA climate variability is well-characterized in the Pyrenees
456 thanks to records from glaciers, such as moraines associated with glacier advances, but also due to historical
457 documents such as pictures or old photographs (Oliva et al., 2018). The available information indicates that
458 the LIA glaciers in the Pyrenees occupied 3366 ha in 1876, just 810 ha in 1984 and these glaciers have lost
459 23.2% of their volume considering only from 2011 to 2020 (Hughes, 2018; Vidaller et al., 2021). In many
460 Pyrenean valleys, more than one moraine belt was assigned to the LIA (García-Ruiz et al., 2014) but,
461 unfortunately, the discontinuous character of these landforms and difficulties in dating them does not allow
462 to resolve the internal pattern of the LIA in the Pyrenees. A recent compilation of records across the Iberian
463 mountains proposed several climate phases during the LIA (Oliva et al., 2018), which are well-correlated
464 with our speleothem composite (Fig. 4a): A first cooling phase lasted from the onset of the LIA (ca. 1200
465 CE) until 1480 CE, followed by relatively warmer conditions from 1480 to 1570 CE. A second phase of
466 gradual cooling occurred until 1600 CE followed by very cool conditions lasting until 1715 CE and
467 coinciding with the Maunder Minimum (1645 – 1715CE). In our speleothem composite, this interval is
468 well defined as a cold period but it was not the one with minimum $\delta^{18}\text{O}$ values of the LIA (Fig. 4a). The
469 first half of the 18th century was characterized by warm conditions, supported by many records compiled
470 by Oliva et al. (2018). After 1760 and until the end of the LIA (ca. 1850 CE), a climate deterioration and

471 more frequent extreme climate events were described. This last cold phase is also captured by the
472 speleothem composite and may correspond to the Dalton Minimum (1790 – 1830 CE). It is characterised
473 by large climate variability and lasted until about 1850 CE.

474 E. The Industrial Era in the Pyrenees. The Industrial Era (IE), defined as the last 150 years, is characterized
475 in the Pyrenean speleothem composite by low temperatures that started to increase at about 1950 CE (Fig.
476 4a), in response to the Great Acceleration (Steffen et al., 2015) (yellow band in Fig.4). This increase of
477 temperature is well recorded in other Pyrenean climate archives, such as glaciers or lake records. Thus, the
478 last 150 years were marked by a gradual glacier retreat since 1850 CE that accelerated specially after 1980
479 CE, considered as a “tipping point” in glacier retreat not only on a Pyrenean scale (López-Moreno et al.,
480 2016) but also on a global scale (Beniston et al., 2018). A decrease in heavy rainfall (Fig. 4b) and an increase
481 in salinity (Fig. 4c) are well defined in Montcortés and Estanya lake records, respectively, during the IE,
482 indicating a decrease in precipitation in a, likely, drier scenario. Besides these two lake records, high-
483 altitude lakes show a significant increase in primary productivity during the last decades (Vicente de Vera
484 García et al., 2023). These recent results demonstrate the combined impacts of climate change and increased
485 human pressure in the Pyrenees. Coherently, last 50 years are characterized by generally enriched $\delta^{18}\text{O}$
486 values in our speleothem record (yellow bands in Fig. 4). However, the last two decades (our record ends
487 in 2013, the year XEV sample was collected) are not the ones with the highest $\delta^{18}\text{O}$ values (Fig. 4a) as also
488 observed in tree-ring data from the Spanish Central Pyrenees (Büntgen et al., 2017) (Fig. 4e). One potential
489 explanation for the lack of exceptionally high $\delta^{18}\text{O}$ values would be a slight increase in precipitation
490 amount. Thus, precipitation reconstruction for the Pyrenees during the last two decades indicate slightly
491 higher values than those of previous decades (Pérez-Zanón et al., 2017, Fig. A.5). Other factors, such as
492 changes in the precipitation source or type (eg. dominance of Atlantic frontal rainfall versus Mediterranean
493 convective episodes) may be also behind the recorded $\delta^{18}\text{O}$ values of last decades.

494 **5.2.2. Temperature variability in W Europe and the W Mediterranean during last 2500 years**

495 The PAGES2k European temperature record is the most recent compilation of the last two millennia at
496 European scale (PAGES 2k Consortium, 2013) and it is coherent with our speleothem composite for the
497 Central Pyrenees (Fig. 6). This comparison shows a synchronicity for several of the warmest intervals of
498 the CE, such as the first centuries CE in the RP, the 1150-1250 CE period within the MCA, and the last
499 decades (marked as orange bars in Fig. 6). There are very few high-resolution speleothem records in Europe
500 covering the CE (Comas-Bru et al., 2020); we selected nine speleothems records in Europe and northern
501 Africa which cover with robust chronology and decadal resolution the last 2500 years (Fig. 5). One of these
502 records is interpreted as NAO variability (Baker et al., 2015), three are paleo-precipitation reconstructions
503 (Ait Brahim et al., 2019; Cisneros et al., 2021; Thatcher et al., 2022) and the other five are reflecting paleo-
504 temperature variations (Affolter et al., 2019; Fohlmeyer et al., 2012; Mangini et al., 2005; Martín-Chivelet
505 et al., 2011; Sundqvist et al., 2010). Considering these differences in the interpretation and the fact these
506 records are from different regions with different climates (from Sweden to Morocco), dissimilar profiles of
507 paleoclimate variability can be expected. Still, some features are comparable and can be discussed to obtain
508 a super-regional picture.

509 A. The Roman period in Europe-W Mediterranean. In Europe, and particularly in the Mediterranean region,
510 the RP is well-known as a warm period (e.g., McCormick et al., 2012). The average sea-surface temperature
511 in the western Mediterranean Sea was 2°C higher than the average temperature of the late centuries
512 (Margaritelli et al., 2020). Our composite, with high values of normalized $\delta^{18}\text{O}$ values during the whole
513 RP, and particularly from 0-200 CE, agrees with the scenario of warm temperatures (Fig. 5i). Speleothem
514 data from the Balearic Islands (Cisneros et al., 2021) indicate a transition from humid to dry conditions
515 along the Iberian-RP (Fig. 5c). The dry period at the end of the RP in the Balearic record, appears in
516 agreement with a new speleothem record from northern Italy (Hu et al., 2022), suggesting that the observed
517 drying trend was a possible contribution to the collapse of the Roman Empire in 476 CE. Record from
518 Morocco (Ait Brahim et al., 2019), contrarily, marks a humid trend at the end of the RP (Fig. 5d). Similarly,
519 an increase in humidity was observed in southern Iberia during the RP (Jiménez-Moreno et al., 2013;

520 Martín-Puertas et al., 2009) thus reflecting a large spatial heterogeneity in precipitation when comparing
521 records from the north and south of the Mediterranean basin.

522 B. The Dark Ages in Europe-W Mediterranean. After the RP, the cold Dark Ages started (450-850 CE).
523 Part of this period is known as the “Late Antique Little Ice Age” (LALIA), lasting from 536 CE to 670 CE,
524 characterized by specially cold conditions in Europe (Büntgen et al., 2016). Our speleothem composite
525 shows in general cold-wet conditions, but with centennial-scale variability during the DA (Fig. 5). Three
526 clear intervals can be defined, following the $\delta^{18}\text{O}$ pattern of our composite, as well as speleothem records
527 from the Alps (Mangini et al., 2005) and Central Europe (Affolter et al., 2019; Fohlmeister et al., 2012): an
528 initial cooling phase corresponding to the LALIA (ca. 500-650 CE), a warming phase (ca. 650-750 CE)
529 and a final cooling phase right before the onset of the warming associated with the MCA (ca 750-850 CE).
530 A $\delta^{13}\text{C}$ speleothem record from three N Iberian caves (Martín-Chivelet et al., 2011) shows a warming trend
531 in the DA period but with internal variability that, within dating uncertainties, can be related to the three
532 phases defined above (Fig. 5i). It is worth noting that the period with the most negative $\delta^{18}\text{O}$ values recorded
533 in the speleothem composite from the Pyrenees corresponds to the LALIA decades, a cooling period which
534 provoked widespread social disruption in Europe, famine, and episodes of epidemic diseases (Peregrine,
535 2020).

536 C. The Medieval Climate Anomaly in Europe-W Mediterranean. The MCA was one of the warmest periods
537 in continental Europe (and the W Mediterranean, Lüning et al., 2019) of the CE, usually dated to 900 CE
538 to 1300 CE and characterized by warm (Goosse et al., 2012) and relatively dry conditions (Helama et al.,
539 2009). The MCA was also characterized by a general glacier retreat, mainly associated with a decline in
540 precipitation in the Alps (Holzhauser et al., 2016) and the Pyrenees (Moreno et al., 2021b). This scenario
541 is supported by speleothem records from Europe and the W Mediterranean (Fig. 5), which all point to
542 generally warm (Affolter et al., 2019; Fohlmeister et al., 2012; Mangini et al., 2005; Martín-Chivelet et al.,
543 2011; Sundqvist et al., 2010) and/or dry conditions (Ait Brahim et al., 2019; Baker et al., 2015; Thatcher et
544 al., 2022), even leading to speleothem growth stops as for example seen in the Balearic record (Cisneros et
545 al., 2021). Previous studies have emphasized the complexity of the spatial and seasonal structure of the
546 MCA in Europe (Goosse et al., 2012). The selected speleothem records underscore this complexity,
547 particularly considering that in our Pyrenean composite one of the periods marked as cold-wet occurred
548 during the MCA, ca. 950-1050 CE (Fig. 5). We propose that this cold interval represents the climate
549 response to the Oort solar minimum in the Pyrenees, a time period characterized by low number of sunspots
550 covering spanning 1010 to 1050 CE (Bard et al., 2000).

551 D. The Little Ice Age in Europe-W Mediterranean. The LIA is well known in Europe and the W
552 Mediterranean region, characterized by cold temperatures and relatively humid conditions as recorded, for
553 example, in chironomid-inferred summer temperatures (Ilyashuk et al., 2019), Mediterranean SSTs
554 (Cisneros et al., 2016), the advance of alpine glaciers (Holzhauser et al., 2016) and the rise of lake levels
555 (Magny, 2013). The LIA cooling, however, was not continuous and uniform in space and time. Regarding
556 temperatures, many of the available reconstructions from the Alps (Trachsel et al., 2012), Scandinavia
557 (Zawiska et al., 2017), and other regions of Europe (Luterbacher et al., 2016), provide evidence for a main
558 LIA cooling phase which was divided into three parts: two cold intervals with a slightly warmer episode in
559 between, with the most severe cooling during the 18th century (Ilyashuk et al., 2019). This pattern is also
560 found in the two temperature records from Iberian speleothems (this study and the one from Martín-
561 Chivelet et al., 2011) and a temperature record from the Alps (Mangini et al., 2005) (Fig. 5, marked by
562 arrows). The other European speleothem records show only two phases during the LIA: a longer and intense
563 cooling period followed by a warming (Fig. 5, Affolter et al., 2019; Fohlmeister et al., 2012; Sundqvist et
564 al., 2010). A tripartite pattern is recorded by humidity-sensitive speleothems from Portugal, with wet-dry-
565 wet conditions in excellent agreement with the cold-warm-cold pattern in the Pyrenean record (this study),
566 supporting the concept that this pattern is controlled by changes in intensity and N-S migration of the Azores
567 High (Thatcher et al., 2022).

568 E. The Industrial Era in Europe-W Mediterranean. Between about 1870 CE and today, an increase in
569 temperature is detected by European speleothem records (Fig. 5), as previously shown by the retreat of
570 European glaciers (Beniston et al., 2018) and tree-ring summer temperature records (Büntgen et al., 2011)
571 as well as drought reconstructions (Büntgen et al., 2021). The impacts in Europe and the W Mediterranean
572 of the current global warming trend, accelerated during last 50 years, are becoming more and more evident
573 (Jacob et al., 2018; Naumann et al., 2021).

574 **5.2.3 Drivers of past temperature variability in the Pyrenees**

575 The good correlation and synchronicity between the PAGES2k European record and the Pyrenean
576 composite (marked as orange bars in Fig. 6) supports the interpretation of temperature being the dominant
577 factor in controlling the speleothem record. This centennial-scale correlation can be extended to a
578 worldwide tree-ring compilation (Sigl et al., 2015) pointing to the presence of common warm periods in
579 the Central Pyrenees. Interestingly, if precipitation was the dominant factor controlling the $\delta^{18}\text{O}$ speleothem
580 composite, it would be difficult to find a common signal at regional or even continental scale, as indicated
581 by the overall good correlation shown in Fig. 6.

582 It is worth to mention the good correlation with several especially cold periods at decadal scale (blue bars
583 in Fig. 6), such as the event at 540-550 CE (registered at 520 CE in the speleothem record) or two cold
584 spikes at 800-850 CE at the end of the DA. We proposed that the cold event at ca. 540 CE (the coldest of
585 the speleothem record) is related to a cataclysmic volcanic eruption that took place in Iceland in 536 CE
586 and spewed ash across the Northern Hemisphere, together with the effect of two other massive eruptions in
587 540 and 547 CE (Fig. 6b, Sigl et al., 2015). An unprecedented, long-lasting and spatially synchronized
588 cooling was observed in European tree-ring records associated with these large volcanic eruptions,
589 corresponding to the LALIA period (Büntgen et al., 2016). Therefore, volcanic events, at least the large
590 ones such that from 536 CE in Iceland, have an effect driving temperature variations in the Pyrenean region.

591 There is also an evident synchrony between the European record and the Pyrenean speleothems in several
592 of the more recent coldest intervals of the MCA and the LIA (dark blue bars in Fig. 6), probably a regional
593 response to minima in solar irradiance as these events correspond to minima in sunspot numbers (Fig. 6c,
594 (Usoskin et al., 2014, 2016): 1010-1050 CE (Oort minimum), 1280-1350 CE (Wolf minimum), 1450-1550
595 CE (Spörer minimum), 1645-1715 CE (Maunder minimum) and 1790-1820 CE (Dalton minimum).
596 Because variations in total solar irradiance are relatively small, on the order of a few tenths of Wm^{-2} , the
597 mechanism that could result in a detectable cooling remains uncertain (Gray et al., 2010). While some
598 studies discarded the idea that there has been a strong direct radiative influence of solar forcing on Northern
599 Hemisphere temperatures in the past millennium (Schurer et al., 2014), other authors demonstrated a
600 connection among solar variability and climate throughout changes in the large-scale atmospheric
601 circulation of the Northern Hemisphere, such as the North Atlantic Oscillation (NAO) (Martin-Puertas et
602 al., 2012). The NAO was proposed as a plausible mechanism to explain climate changes in Europe during
603 the MCA vs LIA periods through the study in combination of proxy records and model simulations (Trouet
604 et al., 2009; Mann et al., 2009). Thus, it was postulated that the MCA/LIA transition included a weakening
605 of the Atlantic Meridional Overturning Circulation (AMOC) and a transition to more negative NAO
606 conditions, resulting in a strong cooling of the North Atlantic region and an increase in the storm intensity
607 (Trouet et al., 2012).

608 Such a connection among solar irradiance and temperature over Europe is then manifested through a change
609 in the pressure gradient in the Atlantic that resembles a negative phase of the NAO and results in lower
610 temperatures over Europe but also in a southward shift of the storm tracks enhancing precipitation over
611 central and southern Europe (Swingedouw et al., 2011). As solar irradiance decreases, colder temperatures
612 over the Northern Hemisphere continents are observed, especially in winter (1° to 2°C), in agreement with
613 historical records and proxy data for surface temperatures (Shindell et al., 2001). Coherently, most episodes
614 of flooding in northwest and northern Europe region match with multi-decadal periods of grand solar
615 minima and are thus also associated to the negative phase in the NAO index (Benito et al., 2015) (Fig. 6d).

616 In Iberia, the NAO forcing was embraced to explain the dryness during the MCA as observed in low
617 resolution records (Moreno et al., 2012). Further studies based on proxy reconstructions in Iberia explained
618 those MCA - LIA differences by using interactions between the NAO and the East Atlantic (EA) phases
619 (Sánchez-López et al., 2016). In that line, the persistence of NAO phases, for example, the dominance of
620 positive index during Medieval times, has been questioned (Ortega et al., 2015) and the interactions with
621 other atmospheric modes, together with the non-stationary character of these atmospheric patterns, are
622 nowadays important issues to contemplate when providing a NAO reconstruction (Comas-Bru and
623 Hernández, 2018). In Fig. 6g, the NAO reconstruction provided using a lake record in NW Iberia
624 (Hernández et al., 2020) is compared with the speleothem Pyrenean record demonstrating a good
625 connection. Not surprisingly, the lack of correlation for some periods could be associated to i) chronological
626 uncertainties of both records, ii) different season recorded by the analyzed proxies and iii) distinct influence
627 of NAO in W and E of the IP.

628 **6. Conclusions**

629 The eight stalagmites presented in this study document for the first-time significant climate changes on the
630 decadal scale in the Central Pyrenees during the last 2500 years. The $\delta^{18}\text{O}$ composite record is dominated
631 by regional temperature changes, as suggested by monitoring data and by the correlation with observational
632 temperature data from the Pyrenees and at a hemispheric scale. The precipitation amount may also play a
633 role as shown by the comparison with Pyrenean lake records.

634 On a regional scale, there is a good agreement with other Pyrenean and Iberian records (lake levels, tree
635 rings and glacier advances) indicating a regional representativity of this new record. The RP stands out as
636 a clear warm period, while the DA, MCA and LIA exhibit a high centennial-scale variability with cold
637 (e.g., 520-540 CE and 1750-1850 CE) and warm intervals (e.g., 900-950 CE and 1150-1250 CE) modulated
638 by increases and decreases in the precipitation amount, respectively. In spite temperature increases since
639 1950 CE, known as the Great Acceleration within the IE, the last two decades are not the ones with the
640 highest $\delta^{18}\text{O}$ values in the composite record, likely pointing to the secondary role played by precipitation
641 amount.

642 On a European scale, the Pyrenean composite is in robust agreement with the PAGES2k temperature
643 reconstructions, particularly during warm events. It shows some similarities with other speleothem
644 reconstructions from the Alps, Central and Northern Europe pointing to coherent patterns all over the
645 continent for cold/wet and warm/dry periods of last 2500 years. This coherence is supported by synchronous
646 changes with the sunspot number (low temperatures during solar minima), the North Atlantic Oscillation
647 index (low NAO correlates with cold and wet decades) and major volcanic eruptions (e.g., several eruptions
648 during LALIA).

649 **Author contribution.** MB, AM and CS designed the study; MB, AB and CS carried out the field work;
650 MB, JH, IC, HS and NH did the analyses. LE and HC provided the U-Th facilities. MB and AM prepared
651 the manuscript with contributions from all co-authors.

652 **Competing interests:** The authors declare that they have no conflict of interest.

653 **Acknowledgements.** We acknowledge the Spanish projects CTM2013-48639-C2-2-R (OPERA),
654 CGL2016-77479-R (SPYRIT), and PID2019-106050RB-I00 (PYCACHU) for funding. We thank the
655 Ordesa y Monte Perdido National Park (Spain) authorities and guards for their permission and help in
656 exploring and monitoring the studied caves. We also thank Jaime Mas and Xavier Fuertes (Free Caving
657 Team and GEB), Ramón Queraltó and Carles Pons (Asociación Científica Espeleológica Cotiella), Maria
658 Leunda and the Palazzo family (www.hotelpalazio.com) for their invaluable help during fieldwork. Dr.
659 Miguel Sevilla (IPE-CSIC) is greatly acknowledge for his design and production of maps in Fig. 1. The
660 authors would like to acknowledge the use of the Servicio General de Apoyo a la Investigación-SAI,
661 University of Zaragoza. This study contributes to the work carried out by the DGA research group Procesos
662 Geoambientales y Cambio Global (ref.: E02-20R). Miguel Bartolomé is supported by the HORIZON TMA

663 MSCA Postdoctoral Fellowships - Global Fellowships 2022 MODKARST project (n° 101107943) funded
664 by the European Union. Isabel Cacho thanks the Catalan Institution for Research and Advanced Studies
665 (ICREA) academia program from the Generalitat de Catalunya.

666 **References**

667 Abrantes, F., Rodrigues, T., Rufino, M., Salgueiro, E., Oliveira, D., Gomes, S., Oliveira, P., Costa,
668 A., Mil-Homens, M., Drago, T., and Naughton, F.: The climate of the Common Era off the
669 Iberian Peninsula, *Clim. Past*, 13, 1901–1918, <https://doi.org/10.5194/cp-13-1901-2017>, 2017.

670 Affolter, S., Häuselmann, A., Fleitmann, D., Edwards, R. L., Cheng, H., and Leuenberger, M.:
671 Central Europe temperature constrained by speleothem fluid inclusion water isotopes over the
672 past 14,000 years, *Science Advances*, 5, eaav3809, <https://doi.org/10.1126/sciadv.aav3809>,
673 2019.

674 Ahmed, M., Anchukaitis, K. J., Asrat, A., Borgaonkar, H. P., Braidia, M., Buckley, B. M., Büntgen,
675 U., Chase, B. M., Christie, D. A., Cook, E. R., Curran, M. A. J., Diaz, H. F., Esper, J., Fan, Z.-X.,
676 Gaire, N. P., Ge, Q., Gergis, J., González-Rouco, J. F., Goosse, H., Grab, S. W., Graham, N.,
677 Graham, R., Grosjean, M., Hanhijärvi, S. T., Kaufman, D. S., Kiefer, T., Kimura, K., Korhola, A. A.,
678 Krusic, P. J., Lara, A., Lézine, A.-M., Ljungqvist, F. C., Lorrey, A. M., Luterbacher, J., Masson-
679 Delmotte, V., McCarroll, D., McConnell, J. R., McKay, N. P., Morales, M. S., Moy, A. D.,
680 Mulvaney, R., Mundo, I. A., Nakatsuka, T., Nash, D. J., Neukom, R., Nicholson, S. E., Oerter, H.,
681 Palmer, J. G., Phipps, S. J., Prieto, M. R., Rivera, A., Sano, M., Severi, M., Shanahan, T. M., Shao,
682 X., Shi, F., Sigl, M., Smerdon, J. E., Solomina, O. N., Steig, E. J., Stenni, B., Thamban, M., Trouet,
683 V., Turney, C. S. M., Umer, M., van Ommen, T., Verschuren, D., Vial, A. E., Villalba, R., Vinther,
684 B. M., von Gunten, L., Wagner, S., Wahl, E. R., Wanner, H., Werner, J. P., White, J. W. C., Yasue,
685 K., Zorita, E., and PAGES 2k Consortium: Continental-scale temperature variability during the
686 past two millennia, *Nature Geoscience*, 6, 339–346, <https://doi.org/10.1038/ngeo1797>, 2013.

687 Ait Brahim, Y., Wassenburg, J. A., Sha, L., Cruz, F. W., Deininger, M., Sifeddine, A., Bouchaou, L.,
688 Spötl, C., Edwards, R. L., and Cheng, H.: North Atlantic Ice-Rafting, Ocean and Atmospheric
689 Circulation During the Holocene: Insights From Western Mediterranean Speleothems,
690 *Geophysical Research Letters*, 46, 7614–7623, <https://doi.org/10.1029/2019GL082405>, 2019.

691 Baker, A., C. Hellstrom, J., Kelly, B. F. J., Mariethoz, G., and Trouet, V.: A composite annual-
692 resolution stalagmite record of North Atlantic climate over the last three millennia, *Sci Rep*, 5,
693 10307, <https://doi.org/10.1038/srep10307>, 2015.

694 Bard, E., Raisbeck, G., Yiou, F., and Jouzel, J.: Solar irradiance during the last 1200 years based
695 on cosmogenic nuclides, *Tellus B*, 52, 985–992, <https://doi.org/10.1034/j.1600-0889.2000.d01-7.x>, 2000.

697 Bartolomé, M.: La Cueva del Caserío de Sesó (Pirineo Central): espeleogénesis, dinámica actual
698 y reconstrucción paleoambiental de los últimos 13.000 años, Universidad de Zaragoza, 276 pp.,
699 2016.

700 Bartolomé, M., Moreno, A., Sancho, C., Stoll, H. M., Cacho, I., Spötl, C., Belmonte, Á., Edwards,
701 R. L., Cheng, H., and Hellstrom, J. C.: Hydrological change in Southern Europe responding to
702 increasing North Atlantic overturning during Greenland Stadial 1, *PNAS*, 112, 6568–6572,
703 <https://doi.org/10.1073/pnas.1503990112>, 2015a.

704 Bartolomé, M., Sancho, C., Moreno, A., Oliva-Urcia, B., Belmonte, Á., Bastida, J., Cheng, H., and
705 Edwards, R. L.: Upper Pleistocene interstratal piping-cave speleogenesis: The Sesó Cave System

- 706 (Central Pyrenees, Northern Spain), *Geomorphology*, 228, 335–344,
707 <https://doi.org/10.1016/j.geomorph.2014.09.007>, 2015b.
- 708 Beniston, M., Farinotti, D., Stoffel, M., Andreassen, L. M., Coppola, E., Eckert, N., Fantini, A.,
709 Giacona, F., Hauck, C., Huss, M., Huwald, H., Lehning, M., López-Moreno, J.-I., Magnusson, J.,
710 Marty, C., Morán-Tejeda, E., Morin, S., Naaim, M., Provenzale, A., Rabatel, A., Six, D., Stötter,
711 J., Strasser, U., Terzago, S., and Vincent, C.: The European mountain cryosphere: a review of its
712 current state, trends, and future challenges, *The Cryosphere*, 12, 759–794,
713 <https://doi.org/10.5194/tc-12-759-2018>, 2018.
- 714 Benito, G., Macklin, M. G., Panin, A., Rossato, S., Fontana, A., Jones, A. F., Machado, M. J.,
715 Matlakhova, E., Mozzi, P., and Zielhofer, C.: Recurring flood distribution patterns related to
716 short-term Holocene climatic variability, *Sci Rep*, 5, 16398, <https://doi.org/10.1038/srep16398>,
717 2015.
- 718 Bernal-Wormull, J. L., Moreno, A., Pérez-Mejías, C., Bartolomé, M., Aranburu, A.,
719 Arriolabengoa, M., Iriarte, E., Cacho, I., Spötl, C., Edwards, R. L., and Cheng, H.: Immediate
720 temperature response in northern Iberia to last deglacial changes in the North Atlantic,
721 *Geology*, <https://doi.org/10.1130/G48660.1>, 2021.
- 722 Bücher, A. and Dessens, J.: Secular Trend of Surface Temperature at an Elevated Observatory
723 in the Pyrenees, *Journal of Climate*, 4, 859–868, [https://doi.org/10.1175/1520-0442\(1991\)004<0859:STOSTA>2.0.CO;2](https://doi.org/10.1175/1520-0442(1991)004<0859:STOSTA>2.0.CO;2), 1991.
- 725 Büntgen, U., Tegel, W., Nicolussi, K., McCormick, M., Frank, D., Trouet, V., Kaplan, J. O., Herzig,
726 F., Heussner, K.-U., Wanner, H., Luterbacher, J., and Esper, J.: 2500 Years of European Climate
727 Variability and Human Susceptibility, *Science*, 2011.
- 728 Büntgen, U., Myglan, V. S., Ljungqvist, F. C., McCormick, M., Di Cosmo, N., Sigl, M., Jungclaus,
729 J., Wagner, S., Krusic, P. J., Esper, J., Kaplan, J. O., de Vaan, M. A. C., Luterbacher, J., Wacker, L.,
730 Tegel, W., and Kiryandov, A. V.: Cooling and societal change during the Late Antique Little Ice
731 Age from 536 to around 660 AD, *Nature Geosci*, 9, 231–236,
732 <https://doi.org/10.1038/ngeo2652>, 2016.
- 733 Büntgen, U., Krusic, P. J., Verstege, A., Sangüesa-Barreda, G., Wagner, S., Camarero, J. J.,
734 Ljungqvist, F. C., Zorita, E., Oppenheimer, C., Konter, O., Tegel, W., Gärtner, H., Cherubini, P.,
735 Reinig, F., and Esper, J.: New Tree-Ring Evidence from the Pyrenees Reveals Western
736 Mediterranean Climate Variability since Medieval Times, *J. Climate*, 30, 5295–5318,
737 <https://doi.org/10.1175/JCLI-D-16-0526.1>, 2017.
- 738 Büntgen, U., Urban, O., Krusic, P. J., Rybníček, M., Kolář, T., Kyncl, T., Ač, A., Koňasová, E.,
739 Čáslavský, J., Esper, J., Wagner, S., Saurer, M., Tegel, W., Dobrovolný, P., Cherubini, P., Reinig,
740 F., and Trnka, M.: Recent European drought extremes beyond Common Era background
741 variability, *Nat. Geosci.*, 14, 190–196, <https://doi.org/10.1038/s41561-021-00698-0>, 2021.
- 742 Cisneros, M., Cacho, I., Frigola, J., Canals, M., Masqué, P., Martrat, B., Casado, M., Grimalt, J.
743 O., Pena, L. D., Margaritelli, G., and Lirer, F.: Sea surface temperature variability in the central-
744 western Mediterranean Sea during the last 2700 years: a multi-proxy and multi-record
745 approach, *Clim. Past*, 12, 849–869, <https://doi.org/10.5194/cp-12-849-2016>, 2016.
- 746 Cisneros, M., Cacho, I., Moreno, A., Stoll, H., Torner, J., Català, A., Edwards, R. L., Cheng, H.,
747 and Fornós, J. J.: Hydroclimate variability during the last 2700 years based on stalagmite multi-

- 748 proxy records in the central-western Mediterranean, *Quaternary Science Reviews*, 269,
749 107137, <https://doi.org/10.1016/j.quascirev.2021.107137>, 2021.
- 750 Comas-Bru, L. and Hernández, A.: Reconciling North Atlantic climate modes: revised monthly
751 indices for the East Atlantic and the Scandinavian patterns beyond the 20th century, *Earth
752 System Science Data*, 10, 2329–2344, <https://doi.org/10.5194/essd-10-2329-2018>, 2018.
- 753 Comas-Bru, L., Rehfeld, K., Roesch, C., Amirnezhad-Mozhdehi, S., Harrison, S. P.,
754 Atsawawaranunt, K., Ahmad, S. M., Brahim, Y. A., Baker, A., Bosomworth, M., Breitenbach, S.
755 F. M., Burstyn, Y., Columbu, A., Deininger, M., Demény, A., Dixon, B., Fohlmeister, J., Hatvani, I.
756 G., Hu, J., Kaushal, N., Kern, Z., Labuhn, I., Lechleitner, F. A., Lorrey, A., Martrat, B., Novello, V.
757 F., Oster, J., Pérez-Mejías, C., Scholz, D., Scroxton, N., Sinha, N., Ward, B. M., Warken, S.,
758 Zhang, H., and SISAL Working Group members: SISALv2: a comprehensive speleothem isotope
759 database with multiple age–depth models, *Earth System Science Data*, 12, 2579–2606,
760 <https://doi.org/10.5194/essd-12-2579-2020>, 2020.
- 761 Corella, J. P., Valero-Garcés, B. L., Vicente-Serrano, S. M., Brauer, A., and Benito, G.: Three
762 millennia of heavy rainfalls in Western Mediterranean: frequency, seasonality and atmospheric
763 drivers, *Scientific Reports*, 6, <https://doi.org/10.1038/srep38206>, 2016.
- 764 Dessens, J. and Bücher, A.: Changes in minimum and maximum temperatures at the Pic du
765 Midi in relation with humidity and cloudiness, 1882–1984, *Atmospheric Research*, 37, 147–
766 162, [https://doi.org/10.1016/0169-8095\(94\)00075-O](https://doi.org/10.1016/0169-8095(94)00075-O), 1995.
- 767 Edwards, R. L., Chen, J. H., and Wasserburg, G. J.: 238U-234U-230Th-232Th systematics and
768 the precise measurements of time over the past 500.000 years, *Earth and Planetary Science
769 Letters*, 81, 175–192, 1987.
- 770 Fohlmeister, J.: A statistical approach to construct composite climate records of dated
771 archives, *Quaternary Geochronology*, 14, 48–56,
772 <https://doi.org/10.1016/j.quageo.2012.06.007>, 2012.
- 773 Fohlmeister, J., Kromer, B., and Mangini, A.: The influence of soil organic matter age spectrum
774 on the reconstruction of atmospheric 14C levels via stalagmites, *Radiocarbon*, 53, 99–115,
775 <https://doi.org/10.1017/S003382220003438X>, 2011.
- 776 Fohlmeister, J., Schröder-Ritzrau, A., Scholz, D., Spötl, C., Riechelmann, D. F. C., Mudelsee, M.,
777 Wackerbarth, A., Gerdes, A., Riechelmann, S., Immenhauser, A., Richter, D. K., and Mangini, A.:
778 Bunker Cave stalagmites: an archive for central European Holocene climate variability, *Clim.
779 Past*, 8, 1751–1764, <https://doi.org/10.5194/cp-8-1751-2012>, 2012.
- 780 García-Ruiz, J. M., Palacios, D., Andrés, N. de, Valero-Garcés, B. L., López-Moreno, J. I., and
781 Sanjuán, Y.: Holocene and ‘Little Ice Age’ glacial activity in the Marboré Cirque, Monte Perdido
782 Massif, Central Spanish Pyrenees, *The Holocene*, 24, 1439–1452,
783 <https://doi.org/10.1177/0959683614544053>, 2014.
- 784 Genty, D., Vokal, B., Obelic, B., and Massault, M.: Bomb 14C time history recorded in two
785 modern stalagmites — importance for soil organic matter dynamics and bomb 14C distribution
786 over continents, *Earth and Planetary Science Letters*, 160, 795–809,
787 [https://doi.org/10.1016/S0012-821X\(98\)00128-9](https://doi.org/10.1016/S0012-821X(98)00128-9), 1998.
- 788 Genty, D., Blamart, D., Ghaleb, B., Plagnes, V., Causse, Ch., Bakalowicz, M., Zouari, K., Chkir, N.,
789 Hellstrom, J., Wainer, K., and Bourges, F.: Timing and dynamics of the last deglaciation from

- 790 European and North African $\delta^{13}\text{C}$ stalagmite profiles—comparison with Chinese and South
791 Hemisphere stalagmites, *Quaternary Science Reviews*, 25, 2118–2142,
792 <https://doi.org/10.1016/j.quascirev.2006.01.030>, 2006.
- 793 Genty, D., Labuhn, I., Hoffmann, G., Danis, P. A., Mestre, O., Bourges, F., Wainer, K., Massault,
794 M., Van Exter, S., Régnier, E., Orengo, Ph., Falourd, S., and Minster, B.: Rainfall and cave water
795 isotopic relationships in two South-France sites, *Geochimica et Cosmochimica Acta*, 131, 323–
796 343, <https://doi.org/10.1016/j.gca.2014.01.043>, 2014.
- 797 Giménez, R., Bartolomé, M., Gázquez, F., Iglesias, M., and Moreno, A.: Underlying Climate
798 Controls in Triple Oxygen (^{16}O , ^{17}O , ^{18}O) and Hydrogen (^1H , ^2H) Isotopes Composition of
799 Rainfall (Central Pyrenees), *Front. Earth Sci.*, 9, <https://doi.org/10.3389/feart.2021.633698>,
800 2021.
- 801 González-Sampériz, P., Aranbarri, J., Pérez-Sanz, A., Gil-Romera, G., Moreno, A., Leunda, M.,
802 Sevilla-Callejo, M., Corella, J. P., Morellón, M., Oliva, B., and Valero-Garcés, B.: Environmental
803 and climate change in the southern Central Pyrenees since the Last Glacial Maximum: A view
804 from the lake records, *CATENA*, 149, 668–688, 2017.
- 805 Goosse, H., Guiot, J., Mann, M. E., Dubinkina, S., and Sallaz-Damaz, Y.: The medieval climate
806 anomaly in Europe: Comparison of the summer and annual mean signals in two
807 reconstructions and in simulations with data assimilation, *Global and Planetary Change*, 84–85,
808 35–47, <https://doi.org/10.1016/j.gloplacha.2011.07.002>, 2012.
- 809 Gray, L. J., Beer, J., Geller, M., Haigh, J. D., Lockwood, M., Matthes, K., Cubasch, U., Fleitmann,
810 D., Harrison, G., Hood, L., Luterbacher, J., Meehl, G. A., Shindell, D., van Geel, B., and White,
811 W.: Solar influences on climate, *Rev. Geophys.*, 48, RG4001, 2010.
- 812 Hammer, O., Harper, D. A. T., and Ryan, P. D.: PAST: Paleontological statistics software package
813 for education and data analysis. 4(1): 9pp., *Palaeontologia Electronica*, 4 (1), 9, 2001.
- 814 Helama, S., Meriläinen, J., and Tuomenvirta, H.: Multicentennial megadrought in northern
815 Europe coincided with a global El Niño–Southern Oscillation drought pattern during the
816 Medieval Climate Anomaly, *Geology*, 37, 175–178, <https://doi.org/10.1130/G25329A.1>, 2009.
- 817 Hellstrom, J.: U–Th dating of speleothems with high initial ^{230}Th using stratigraphical
818 constraint, *Quaternary Geochronology*, 1, 289–295,
819 <https://doi.org/10.1016/j.quageo.2007.01.004>, 2006.
- 820 Hernández, A., Sánchez-López, G., Pla-Rabes, S., Comas-Bru, L., Parnell, A., Cahill, N., Geyer, A.,
821 Trigo, R. M., and Giral, S.: A 2,000-year Bayesian NAO reconstruction from the Iberian
822 Peninsula, *Sci Rep*, 10, 14961, <https://doi.org/10.1038/s41598-020-71372-5>, 2020.
- 823 Holzhauser, H., Magny, M., and Zumbuühl, H. J.: Glacier and lake-level variations in west-
824 central Europe over the last 3500 years:, *The Holocene*,
825 <https://doi.org/10.1191/0959683605hl853ra>, 2016.
- 826 Hu, H.-M., Michel, V., Valensi, P., Mii, H.-S., Starnini, E., Zunino, M., and Shen, C.-C.: Stalagmite-
827 Inferred Climate in the Western Mediterranean during the Roman Warm Period, *Climate*, 10,
828 93, <https://doi.org/10.3390/cli10070093>, 2022.

- 829 Hua, Q., McDonald, J., Redwood, D., Drysdale, R., Lee, S., Fallon, S., and Hellstrom, J.: Robust
830 chronological reconstruction for young speleothems using radiocarbon, *Quaternary*
831 *Geochronology*, 14, 67–80, <https://doi.org/10.1016/j.quageo.2012.04.017>, 2012.
- 832 Hua, Q., Cook, D., Fohlmeister, J., Penny, D., Bishop, P., and Buckman, S.: Radiocarbon Dating
833 of a Speleothem Record of Paleoclimate for Angkor, Cambodia, *Radiocarbon*, 59, 1873–1890,
834 <https://doi.org/10.1017/RDC.2017.115>, 2017.
- 835 Hughes, P. D.: Little Ice Age glaciers and climate in the Mediterranean mountains: a new
836 analysis, *CIG*, 44, 15, <https://doi.org/10.18172/cig.3362>, 2018.
- 837 Ilyashuk, E. A., Heiri, O., Ilyashuk, B. P., Koinig, K. A., and Psenner, R.: The Little Ice Age
838 signature in a 700-year high-resolution chironomid record of summer temperatures in the
839 Central Eastern Alps, *Clim Dyn*, 52, 6953–6967, <https://doi.org/10.1007/s00382-018-4555-y>,
840 2019.
- 841 IPCC, 2021: Climate Change 2021: The Physical Science Basis. Contribution of Working Group I
842 to the Sixth Assessment Report of the Intergovernmental Panel on Climate Change [Masson-
843 Delmotte, V., P. Zhai, A. Pirani, S.L. Connors, C. Péan, S. Berger, N. Caud, Y. Chen, L. Goldfarb,
844 M.I. Gomis, M. Huang, K. Leitzell, E. Lonnoy, J.B.R. Matthews, T.K. Maycock, T. Waterfield, O.
845 Yelekçi, R. Yu, and B. Zhou (eds.)]. Cambridge University Press, Cambridge, United Kingdom
846 and New York, NY, USA, 2391 pp.doi:10.1017/9781009157896.
- 847 Jacob, D., Kotova, L., Teichmann, C., Sobolowski, S. P., Vautard, R., Donnelly, C., Koutroulis, A.
848 G., Grillakis, M. G., Tsanis, I. K., Damm, A., Sakalli, A., and van Vliet, M. T. H.: Climate Impacts in
849 Europe Under +1.5°C Global Warming, *Earth’s Future*, 6, 264–285,
850 <https://doi.org/10.1002/2017EF000710>, 2018.
- 851 Jiménez-Moreno, G., García-Alix, A., Hernández-Corbalán, M. D., Anderson, R. S., and Delgado-
852 Huertas, A.: Vegetation, fire, climate and human disturbance history in the southwestern
853 Mediterranean area during the late Holocene, *Quaternary Research*, 79, 110–122,
854 <https://doi.org/10.1016/j.yqres.2012.11.008>, 2013.
- 855 Konecky, B. L., McKay, N. P., Churakova (Sidorova), O. V., Comas-Bru, L., Dassié, E. P., DeLong,
856 K. L., Falster, G. M., Fischer, M. J., Jones, M. D., Jonkers, L., Kaufman, D. S., Leduc, G.,
857 Managave, S. R., Martrat, B., Opel, T., Orsi, A. J., Partin, J. W., Sayani, H. R., Thomas, E. K.,
858 Thompson, D. M., Tyler, J. J., Abram, N. J., Atwood, A. R., Conroy, J. L., Kern, Z., Porter, T. J.,
859 Stevenson, S. L., von Gunten, L., and the Iso2k Project Members: The Iso2k Database: A global
860 compilation of paleo- $\delta^{18}\text{O}$ and $\delta^2\text{H}$ records to aid understanding of Common Era climate, *Earth*
861 *System Science Data Discussions*, 1–49, <https://doi.org/10.5194/essd-2020-5>, 2020.
- 862 Lachniet, M. S.: Climatic and environmental controls on speleothem oxygen-isotope values,
863 *Quaternary Science Reviews*, 28, 412–432, 2009.
- 864 Leunda, M., González-Sampériz, P., Gil-Romera, G., Bartolomé, M., Belmonte-Ribas, Á., Gómez-
865 García, D., Kaltenrieder, P., Rubiales, J. M., Schwörer, C., Tinner, W., Morales-Molino, C., and
866 Sancho, C.: Ice cave reveals environmental forcing of long-term Pyrenean tree line dynamics,
867 *Journal of Ecology*, 107, 814–828, <https://doi.org/10.1111/1365-2745.13077>, 2019.
- 868 López-Moreno, J. I., Revuelto, J., Rico, I., Chueca-Cía, J., Julián, A., Serreta, A., Serrano, E.,
869 Vicente-Serrano, S. M., Azorin-Molina, C., Alonso-González, E., and García-Ruiz, J. M.: Thinning
870 of the Monte Perdido Glacier in the Spanish Pyrenees since 1981, *The Cryosphere*, 10, 681–
871 694, <https://doi.org/10.5194/tc-10-681-2016>, 2016.

- 872 López-Moreno, J. I., García-Ruiz, J. M., Vicente-Serrano, S. M., Alonso-González, E., Revuelto-
873 Benedí, J., Rico, I., Izagirre, E., and Beguería-Portugués, S.: Critical discussion of: “A farewell to
874 glaciers: Ecosystem services loss in the Spanish Pyrenees,” *Journal of Environmental*
875 *Management*, 275, 111247, <https://doi.org/10.1016/j.jenvman.2020.111247>, 2020.
- 876 Lüning, S., Schulte, L., Garcés-Pastor, S., Danladi, I. b., and Gałka, M.: The Medieval Climate
877 Anomaly in the Mediterranean Region, *Paleoceanography and Paleoclimatology*, 34, 1625–
878 1649, <https://doi.org/10.1029/2019PA003734>, 2019.
- 879 Luterbacher, J., Werner, J. P., Smerdon, J. E., Fernández-Donado, L., González-Rouco, F. J.,
880 Barriopedro, D., Ljungqvist, F. C., Büntgen, U., Zorita, E., Wagner, S., Esper, J., McCarroll, D.,
881 Toreti, A., Frank, D., Jungclaus, J. H., M Barriendos, Bertolin, C., Bothe, O., Brázdil, R., Camuffo,
882 D., Dobrovolný, P., Gagen, M., García-Bustamante, E., Ge, Q., Gómez-Navarro, J. J., Guiot, J.,
883 Hao, Z., Hegerl, G. C., Holmgren, K., Klimenko, V. V., Martín-Chivelet, J., Pfister, C., N Roberts,
884 Schindler, A., Schurer, A., Solomina, O., Gunten, L. von, Wahl, E., Wanner, H., Wetter, O.,
885 Xoplaki, E., Yuan, N., D Zanchettin, Zhang, H., and Zerefos, C.: European summer temperatures
886 since Roman times, *Environ. Res. Lett.*, 11, 024001, [https://doi.org/10.1088/1748-](https://doi.org/10.1088/1748-9326/11/2/024001)
887 [9326/11/2/024001](https://doi.org/10.1088/1748-9326/11/2/024001), 2016.
- 888 Magny, M.: Orbital, ice-sheet, and possible solar forcing of Holocene lake-level fluctuations in
889 west-central Europe: A comment on Bleicher, *The Holocene*,
890 <https://doi.org/10.1177/0959683613483627>, 2013.
- 891 Mangini, A., Spötl, C., and Verdes, P.: Reconstruction of temperature in the Central Alps during
892 the past 2000 yr from a $\delta^{18}\text{O}$ stalagmite record, *Earth and Planetary Science Letters*, 235, 741–
893 751, <https://doi.org/10.1016/j.epsl.2005.05.010>, 2005.
- 894 Mann, M. E.: Beyond the hockey stick: Climate lessons from the Common Era, *PNAS*, 118,
895 <https://doi.org/10.1073/pnas.2112797118>, 2021.
- 896 Mann, M. E., Zhang, Z., Rutherford, S., Bradley, R. S., Hughes, M. K., Shindell, D., Ammann, C.,
897 Faluvegi, G., and Ni, F.: Global Signatures and Dynamical Origins of the Little Ice Age and
898 Medieval Climate Anomaly, *Science*, 326, 1256–1260, 2009.
- 899 Margaritelli, G., Cacho, I., Català, A., Barra, M., Bellucci, L. G., Lubritto, C., Rettori, R., and Lirer,
900 F.: Persistent warm Mediterranean surface waters during the Roman period, *Sci Rep*, 10,
901 10431, <https://doi.org/10.1038/s41598-020-67281-2>, 2020.
- 902 Markowska, M., Fohlmeister, J., Treble, P. C., Baker, A., Andersen, M. S., and Hua, Q.:
903 Modelling the ^{14}C bomb-pulse in young speleothems using a soil carbon continuum model,
904 *Geochimica et Cosmochimica Acta*, 261, 342–367, <https://doi.org/10.1016/j.gca.2019.04.029>,
905 2019.
- 906 Martín-Chivelet, J., Muñoz-García, M. B., Edwards, R. L., Turrero, M. J., and Ortega, A. I.: Land
907 surface temperature changes in Northern Iberia since 4000yrBP, based on $\delta^{13}\text{C}$ of
908 speleothems, *Global and Planetary Change*, 77, 1–12,
909 <https://doi.org/10.1016/j.gloplacha.2011.02.002>, 2011.
- 910 Martín-Puertas, C., Valero-Garcés, B. L., Brauer, A., Mata, M. P., Delgado-Huertas, A., and
911 Dulski, P.: The Iberian-Roman Humid Period (2600-1600 cal yr BP) in the Zoñar Lake varve
912 record (Andalucía, southern Spain), *Quaternary Research*, 71, 108–120, 2009.

- 913 Martin-Puertas, C., Matthes, K., Brauer, A., Muscheler, R., Hansen, F., Petrick, C., Aldahan, A.,
914 Possnert, G., and van Geel, B.: Regional atmospheric circulation shifts induced by a grand solar
915 minimum, *Nature Geoscience*, <https://doi.org/10.1038/ngeo1460>, 2012.
- 916 McCormick, M., Büntgen, U., Cane, M. A., Cook, E. R., Harper, K., Huybers, P., Litt, T., Manning,
917 S. W., Mayewski, P. A., More, A. F. M., Nicolussi, K., and Tegel, W.: Climate Change during and
918 after the Roman Empire: Reconstructing the Past from Scientific and Historical Evidence, *The
919 Journal of Interdisciplinary History*, 43, 169–220, https://doi.org/10.1162/JINH_a_00379, 2012.
- 920 Morellón, M., Valero-Garcés, B., Vegas-Vilarrúbia, T., González-Sampériz, P., Romero, Ó.,
921 Delgado-Huertas, A., Mata, P., Moreno, A., Rico, M., and Corella, J. P.: Lateglacial and Holocene
922 palaeohydrology in the western Mediterranean region: The Lake Estanya record (NE Spain),
923 *Quaternary Science Reviews*, 28, 2582–2599, 2009.
- 924 Morellón, M., Valero-Garcés, B., González-Sampériz, P., Vegas-Vilarrúbia, T., Rubio, E.,
925 Rieradevall, M., Delgado-Huertas, A., Mata, P., Romero, Ó., Engstrom, D. R., López-Vicente, M.,
926 Navas, A., and Soto, J.: Climate changes and human activities recorded in the sediments of
927 Lake Estanya (NE Spain) during the Medieval Warm Period and Little Ice Age, *Journal of
928 Paleolimnology*, 46, 423–452, <https://doi.org/10.1007/s10933-009-9346-3>, 2011.
- 929 Morellón, M., Pérez-Sanz, A., Corella, J. P., Büntgen, U., Catalán, J., González-Sampériz, P.,
930 González-Trueba, J. J., López-Sáez, J. A., Moreno, A., Pla-Rabes, S., Saz-Sánchez, M. Á.,
931 Scussolini, P., Serrano, E., Steinhilber, F., Stefanova, V., Vegas-Vilarrúbia, T., and Valero-Garcés,
932 B.: A multi-proxy perspective on millennium-long climate variability in the Southern Pyrenees,
933 *Clim. Past*, 8, 683–700, <https://doi.org/10.5194/cp-8-683-2012>, 2012.
- 934 Moreno, A., Stoll, H. M., Jiménez-Sánchez, M., Cacho, I., Valero-Garcés, B., Ito, E., and Edwards,
935 L. R.: A speleothem record of rapid climatic shifts during last glacial period from Northern
936 Iberian Peninsula, *Global and Planetary Change*, 71, 218–231;
937 doi:10.1016/j.gloplacha.2009.10.002, 2010.
- 938 Moreno, A., Pérez, A., Frigola, J., Nieto-Moreno, V., Rodrigo-Gámiz, M., Martrat, B., González-
939 Sampériz, P., Morellón, M., Martín-Puertas, C., Corella, J. P., Belmonte, Á., Sancho, C., Cacho, I.,
940 Herrera, G., Canals, M., Grimalt, J. O., Jiménez-Espejo, F., Martínez-Ruiz, F., Vegas-Vilarrúbia,
941 T., and Valero-Garcés, B. L.: The Medieval Climate Anomaly in the Iberian Peninsula
942 reconstructed from marine and lake records, *Quaternary Science Reviews*, 43, 16–32,
943 <https://doi.org/10.1016/j.quascirev.2012.04.007>, 2012.
- 944 Moreno, A., Sancho, C., Bartolomé, M., Oliva-Urcia, B., Delgado-Huertas, A., Estrela, M. J.,
945 Corell, D., López-Moreno, J. I., and Cacho, I.: Climate controls on rainfall isotopes and their
946 effects on cave drip water and speleothem growth: the case of Molinos cave (Teruel, NE
947 Spain), *Clim Dyn*, 43, 221–241, <https://doi.org/10.1007/s00382-014-2140-6>, 2014.
- 948 Moreno, A., Pérez-Mejías, C., Bartolomé, M., Sancho, C., Cacho, I., Stoll, H., Delgado-Huertas,
949 A., Hellstrom, J., Edwards, R. L., and Cheng, H.: New speleothem data from Molinos and Ejulve
950 caves reveal Holocene hydrological variability in northeast Iberia, *Quaternary Research*, 1–11,
951 <https://doi.org/10.1017/qua.2017.39>, 2017.
- 952 Moreno, A., Iglesias, M., Azorin-Molina, C., Pérez-Mejías, C., Bartolomé, M., Sancho, C., Stoll,
953 H., Cacho, I., Frigola, J., Osácar, C., Muñoz, A., Delgado-Huertas, A., Blade, I., and Vimeux, F.:
954 Spatial variability of northern Iberian rainfall stable isotope values: Investigating climatic
955 controls on daily and monthly timescales, *Atmospheric Chemistry and Physics Discussions*, 1–
956 34, <https://doi.org/10.5194/acp-2020-861>, 2021a.

957 Moreno, A., Bartolomé, M., López-Moreno, J. I., Pey, J., Corella, J. P., García-Orellana, J.,
958 Sancho, C., Leunda, M., Gil-Romera, G., González-Sampériz, P., Pérez-Mejías, C., Navarro, F.,
959 Otero-García, J., Lapazaran, J., Alonso-González, E., Cid, C., López-Martínez, J., Oliva-Urcia, B.,
960 Faria, S. H., Sierra, M. J., Millán, R., Querol, X., Alastuey, A., and García-Ruíz, J. M.: The case of a
961 southern European glacier which survived Roman and medieval warm periods but is
962 disappearing under recent warming, *The Cryosphere*, 15, 1157–1172,
963 <https://doi.org/10.5194/tc-15-1157-2021>, 2021b.

964 Morice, C. P., Kennedy, J. J., Rayner, N. A., Winn, J. P., Hogan, E., Killick, R. E., Dunn, R. J. H.,
965 Osborn, T. J., Jones, P. D., and Simpson, I. R.: An Updated Assessment of Near-Surface
966 Temperature Change From 1850: The HadCRUT5 Data Set, *Journal of Geophysical Research:*
967 *Atmospheres*, 126, e2019JD032361, <https://doi.org/10.1029/2019JD032361>, 2021.

968 Naumann, G., Cammalleri, C., Mentaschi, L., and Feyen, L.: Increased economic drought
969 impacts in Europe with anthropogenic warming, *Nat. Clim. Chang.*, 11, 485–491,
970 <https://doi.org/10.1038/s41558-021-01044-3>, 2021.

971 Neukom, R., Steiger, N., Gómez-Navarro, J. J., Wang, J., and Werner, J. P.: No evidence for
972 globally coherent warm and cold periods over the preindustrial Common Era, *Nature*, 571,
973 550–554, <https://doi.org/10.1038/s41586-019-1401-2>, 2019.

974 Observatorio Pirenaico de Cambio Global: Executive summary report OPCC2: Climate change in
975 the Pyrenees: impacts, vulnerability and adaptation, 2018.

976 Oliva, M., Ruiz-Fernández, J., Barriendos, M., Benito, G., Cuadrat, J. M., Domínguez-Castro, F.,
977 García-Ruiz, J. M., Giralt, S., Gómez-Ortiz, A., Hernández, A., López-Costas, O., López-Moreno,
978 J. I., López-Sáez, J. A., Martínez-Cortizas, A., Moreno, A., Prohom, M., Saz, M. A., Serrano, E.,
979 Tejedor, E., Trigo, R., Valero-Garcés, B., and Vicente-Serrano, S. M.: The Little Ice Age in Iberian
980 mountains, *Earth-Science Reviews*, 177, 175–208,
981 <https://doi.org/10.1016/j.earscirev.2017.11.010>, 2018.

982 Ortega, P., Lehner, F., Swingedouw, D., Masson-Delmotte, V., Raible, C. C., Casado, M., and
983 Yiou, P.: A model-tested North Atlantic Oscillation reconstruction for the past millennium,
984 *Nature*, 523, 71–74, <https://doi.org/10.1038/nature14518>, 2015.

985 PAGES 2k Consortium: Continental-scale temperature variability during the past two millennia,
986 *Nature Geosci*, 6, 339–346, <https://doi.org/10.1038/ngeo1797>, 2013.

987 PAGES Hydro2k Consortium: Comparing proxy and model estimates of hydroclimate variability
988 and change over the Common Era, *Climate of the Past*, 13, 1851–1900,
989 <https://doi.org/10.5194/cp-13-1851-2017>, 2017.

990 PAGES2k Consortium, Emile-Geay, J., McKay, N. P., Kaufman, D. S., Gunten, L. von, Wang, J.,
991 Anchukaitis, K. J., Abram, N. J., Addison, J. A., Curran, M. A. J., Evans, M. N., Henley, B. J., Hao,
992 Z., Martrat, B., McGregor, H. V., Neukom, R., Pederson, G. T., Stenni, B., Thirumalai, K.,
993 Werner, J. P., Xu, C., Divine, D. V., Dixon, B. C., Gergis, J., Mundo, I. A., Nakatsuka, T., Phipps, S.
994 J., Routson, C. C., Steig, E. J., Tierney, J. E., Tyler, J. J., Allen, K. J., Bertler, N. A. N., Björklund, J.,
995 Chase, B. M., Chen, M.-T., Cook, E., Jong, R. de, DeLong, K. L., Dixon, D. A., Ekaykin, A. A., Ersek,
996 V., Filipsson, H. L., Francus, P., Freund, M. B., Frezzotti, M., Gaire, N. P., Gajewski, K., Ge, Q.,
997 Goosse, H., Gornostaeva, A., Grosjean, M., Horiuchi, K., Hormes, A., Husum, K., Isaksson, E.,
998 Kandasamy, S., Kawamura, K., Kilbourne, K. H., Koç, N., Leduc, G., Linderholm, H. W., Lorrey, A.
999 M., Mikhailenko, V., Mortyn, P. G., Motoyama, H., Moy, A. D., Mulvaney, R., Munz, P. M., Nash,
1000 D. J., Oerter, H., Opel, T., Orsi, A. J., Ovchinnikov, D. V., Porter, T. J., Roop, H. A., Saenger, C.,

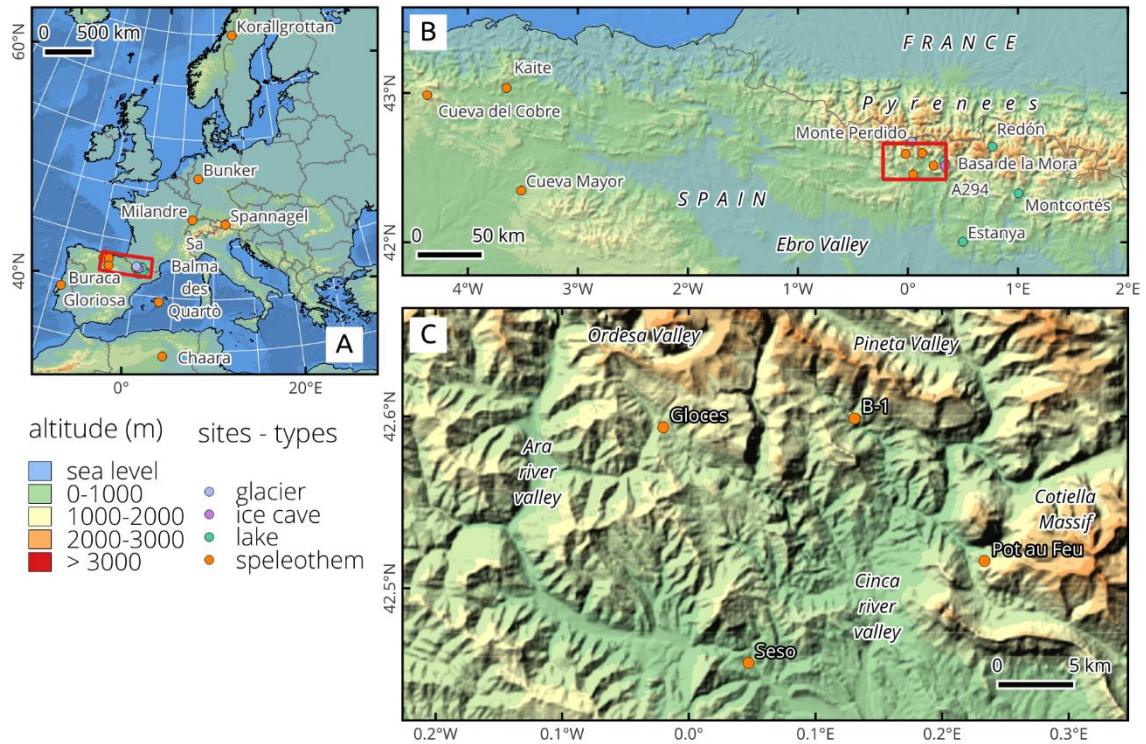
- 1001 Sano, M., Sauchyn, D., Saunders, K. M., Seidenkrantz, M.-S., Severi, M., Shao, X., Sicre, M.-A.,
 1002 Sigl, M., Sinclair, K., George, S. S., Jacques, J.-M. S., Thamban, M., Thapa, U. K., Thomas, E. R.,
 1003 Turney, C., Uemura, R., Viau, A. E., Vladimirova, D. O., Wahl, E. R., White, J. W. C., Yu, Z., and
 1004 Zinke, J.: A global multiproxy database for temperature reconstructions of the Common Era,
 1005 *Scientific Data*, 4, sdata201788, <https://doi.org/10.1038/sdata.2017.88>, 2017.
- 1006 Peregrine, P. N.: Climate and social change at the start of the Late Antique Little Ice Age, *The*
 1007 *Holocene*, 30, 1643–1648, <https://doi.org/10.1177/0959683620941079>, 2020.
- 1008 Pérez-Mejías, C., Moreno, A., Sancho, C., Bartolomé, M., Stoll, H., Osácar, M. C., Cacho, I., and
 1009 Delgado-Huertas, A.: Transference of isotopic signal from rainfall to dripwaters and farmed
 1010 calcite in Mediterranean semi-arid karst, *Geochimica et Cosmochimica Acta*, 243, 66–98,
 1011 <https://doi.org/10.1016/j.gca.2018.09.014>, 2018.
- 1012 Pérez-Zanón, N., Sigró, J., and Ashcroft, L.: Temperature and precipitation regional climate
 1013 series over the central Pyrenees during 1910–2013, *International Journal of Climatology*, 37,
 1014 1922–1937, <https://doi.org/10.1002/joc.4823>, 2017.
- 1015 Pla, S. and Catalan, J.: Chrysophyte cysts from lake sediments reveal the submillennial
 1016 winter/spring climate variability in the northwestern Mediterranean region throughout the
 1017 Holocene, *Climate Dynamics*, 24, 263–278, <https://doi.org/10.1007/s00382-004-0482-1>, 2005.
- 1018 Pla-Rabes, S. and Catalan, J.: Deciphering chrysophyte responses to climate seasonality, *J*
 1019 *Paleolimnol*, 46, 139, <https://doi.org/10.1007/s10933-011-9529-6>, 2011.
- 1020 Priestley, S. C., Treble, P. C., Griffiths, A. D., Baker, A., Abram, N. J., and Meredith, K. T.: Caves
 1021 demonstrate decrease in rainfall recharge of southwest Australian groundwater is
 1022 unprecedented for the last 800 years, *Commun Earth Environ*, 4, 1–12,
 1023 <https://doi.org/10.1038/s43247-023-00858-7>, 2023.
- 1024 Reimer, P.: Discussion: Reporting and Calibration of Post-Bomb 14C Data, *Radiocarbon*, 46,
 1025 1299–1304, <https://doi.org/10.1017/S0033822200033154>, 2004.
- 1026 Rico, I., Izagirre, E., Serrano, E., and López-Moreno, J. I.: Superficie glaciar actual en los
 1027 Pirineos: Una actualización para 2016, *Pirineos*, 172, 029,
 1028 <https://doi.org/10.3989/Pirineos.2017.172004>, 2017.
- 1029 Sánchez-López, G., Hernández, A., Pla-Rabes, S., Trigo, R. M., Toro, M., Granados, I., Sáez, A.,
 1030 Masqué, P., Pueyo, J. J., Rubio-Inglés, M. J., and Giral, S.: Climate reconstruction for the last
 1031 two millennia in central Iberia: The role of East Atlantic (EA), North Atlantic Oscillation (NAO)
 1032 and their interplay over the Iberian Peninsula, *Quaternary Science Reviews*, 149, 135–150,
 1033 <https://doi.org/10.1016/j.quascirev.2016.07.021>, 2016.
- 1034 Sancho, C., Belmonte, Á., Bartolomé, M., Moreno, A., Leunda, M., and López-Martínez, J.:
 1035 Middle-to-late Holocene palaeoenvironmental reconstruction from the A294 ice-cave record
 1036 (Central Pyrenees, northern Spain), *Earth and Planetary Science Letters*, 484, 135–144,
 1037 <https://doi.org/10.1016/j.epsl.2017.12.027>, 2018.
- 1038 Scholz, D. and Hoffmann, D. L.: StalAge - An algorithm designed for construction of speleothem
 1039 age models, *Quaternary Geochronology*, 6, 369–382,
 1040 <https://doi.org/10.1016/j.quageo.2011.02.002>, 2011.

- 1041 Schurer, A. P., Tett, S. F. B., and Hegerl, G. C.: Small influence of solar variability on climate
1042 over the past millennium, *Nature Geosci*, 7, 104–108, <https://doi.org/10.1038/ngeo2040>,
1043 2014.
- 1044 Shen, C. C., Edwards, R. L., Cheng, H., Dorale, J. A., Thomas, R. B., Moran, S. B., Weinstein, S. E.,
1045 and Edmonds, H. N.: Uranium and thorium isotopic and concentration measurements by
1046 magnetic sector inductively coupled plasma mass spectrometry, *Chemical Geology*, 185, 165–
1047 178, 2002.
- 1048 Shindell, D. T., Schmidt, G. A., Mann, M. E., Rind, D., and Waple, A.: benito, *Science*, 294, 2149,
1049 2001.
- 1050 Sigl, M., Winstrup, M., McConnell, J. R., Welten, K. C., Plunkett, G., Ludlow, F., Büntgen, U.,
1051 Caffee, M., Chellman, N., Dahl-Jensen, D., Fischer, H., Kipfstuhl, S., Kostick, C., Maselli, O. J.,
1052 Mekhaldi, F., Mulvaney, R., Muscheler, R., Pasteris, D. R., Pilcher, J. R., Salzer, M., Schüpbach,
1053 S., Steffensen, J. P., Vinther, B. M., and Woodruff, T. E.: Timing and climate forcing of volcanic
1054 eruptions for the past 2,500 years, *Nature*, 523, 543–549,
1055 <https://doi.org/10.1038/nature14565>, 2015.
- 1056 Spötl, C.: Long-term performance of the Gasbench isotope ratio mass spectrometry system for
1057 the stable isotope analysis of carbonate microsamples, *Rapid Commun. Mass Spectrom.*, 25,
1058 1683–1685, <https://doi.org/10.1002/rcm.5037>, 2011.
- 1059 Steffen, W., Broadgate, W., Deutsch, L., Gaffney, O., and Ludwig, C.: The trajectory of the
1060 Anthropocene: The Great Acceleration, *The Anthropocene Review*, 2, 81–98,
1061 <https://doi.org/10.1177/2053019614564785>, 2015.
- 1062 Sundqvist, H. S., Holmgren, K., Moberg, A., Spötl, C., and Mangini, A.: Stable isotopes in a
1063 stalagmite from NW Sweden document environmental changes over the past 4000 years,
1064 *Boreas*, 39, 77–86, <https://doi.org/10.1111/j.1502-3885.2009.00099.x>, 2010.
- 1065 Swingedouw, D., Terray, L., Cassou, C., Voldoire, A., Salas-Melia, D., and Servonnat, J.: Natural
1066 forcing of climate during the last millennium: fingerprint of solar variability, *Climate Dynamics*,
1067 36, 1349–1364, <https://doi.org/10.1007/s00382-010-0803-5>, 2011.
- 1068 Tadros, C. V., Markowska, M., Treble, P. C., Baker, A., Frisia, S., Adler, L., and Drysdale, R. N.:
1069 Recharge variability in Australia’s southeast alpine region derived from cave monitoring and
1070 modern stalagmite $\delta^{18}\text{O}$ records, *Quaternary Science Reviews*, 295, 107742,
1071 <https://doi.org/10.1016/j.quascirev.2022.107742>, 2022.
- 1072 Thatcher, D. L., Wanamaker, A. D., Denniston, R. F., Ummenhofer, C. C., Asmerom, Y., Polyak,
1073 V. J., Cresswell-Clay, N., Hasiuk, F., Haws, J., and Gillikin, D. P.: Iberian hydroclimate variability
1074 and the Azores High during the last 1200 years: evidence from proxy records and climate
1075 model simulations, *Clim Dyn*, <https://doi.org/10.1007/s00382-022-06427-6>, 2022.
- 1076 Trachsel, M., Kamenik, C., Grosjean, M., McCarroll, D., Moberg, A., Brázdil, R., Büntgen, U.,
1077 Dobrovolný, P., Esper, J., Frank, D. C., Friedrich, M., Glaser, R., Larocque-Tobler, I., Nicolussi, K.,
1078 and Riemann, D.: Multi-archive summer temperature reconstruction for the European Alps,
1079 AD 1053–1996, *Quaternary Science Reviews*, 46, 66–79,
1080 <https://doi.org/10.1016/j.quascirev.2012.04.021>, 2012.
- 1081 Treble, P. C., Baker, A., Abram, N. J., Hellstrom, J. C., Crawford, J., Gagan, M. K., Borsato, A.,
1082 Griffiths, A. D., Bajo, P., Markowska, M., Priestley, S. C., Hankin, S., and Paterson, D.:

- 1083 Ubiquitous karst hydrological control on speleothem oxygen isotope variability in a global
1084 study, *Commun Earth Environ*, 3, 1–10, <https://doi.org/10.1038/s43247-022-00347-3>, 2022.
- 1085 Tremaine, D. M., Froelich, P. N., and Wang, Y.: Speleothem calcite farmed in situ: Modern
1086 calibration of $\delta^{18}\text{O}$ and $\delta^{13}\text{C}$ paleoclimate proxies in a continuously-monitored natural cave
1087 system, *Geochimica et Cosmochimica Acta*, 75, 4929–4950,
1088 <https://doi.org/10.1016/j.gca.2011.06.005>, 2011.
- 1089 Trouet, V., Esper, J., Graham, N. E., Baker, A., Scourse, J. D., and Frank, D. C.: Persistent Positive
1090 North Atlantic Oscillation Mode Dominated the Medieval Climate Anomaly, *Science*, 324, 78–
1091 80, 2009.
- 1092 Trouet, V., Scourse, J. D., and Raible, C. C.: North Atlantic storminess and Atlantic Meridional
1093 Overturning Circulation during the last Millennium: Reconciling contradictory proxy records of
1094 NAO variability, *Global and Planetary Change*, 84–85, 48–55,
1095 <https://doi.org/10.1016/j.gloplacha.2011.10.003>, 2012.
- 1096 Usoskin, I. G., Hulot, G., Gallet, Y., Roth, R., Licht, A., Joos, F., Kovaltsov, G. A., Thébault, E., and
1097 Khokhlov, A.: Evidence for distinct modes of solar activity, *A&A*, 562, L10,
1098 <https://doi.org/10.1051/0004-6361/201423391>, 2014.
- 1099 Usoskin, I. G., Gallet, Y., Lopes, F., Kovaltsov, G. A., and Hulot, G.: Solar activity during the
1100 Holocene: the Hallstatt cycle and its consequence for grand minima and maxima, *A&A*, 587,
1101 A150, <https://doi.org/10.1051/0004-6361/201527295>, 2016.
- 1102 Vegas-Vilarrúbia, T., Corella, J. P., Sigró, J., Rull, V., Dorado-Liñan, I., Valero-Garcés, B., and
1103 Gutiérrez-Merino, E.: Regional precipitation trends since 1500 CE reconstructed from calcite
1104 sublayers of a varved Mediterranean lake record (Central Pyrenees), *Science of The Total
1105 Environment*, 826, 153773, <https://doi.org/10.1016/j.scitotenv.2022.153773>, 2022.
- 1106 Vicente de Vera García, A., Mata-Campo, M. P., Pla, S., Vicente, E., Prego, R., Frugone-Álvarez,
1107 M., Polanco-Martínez, J., Galofré, M., and Valero-Garcés, B. L.: Unprecedented recent regional
1108 increase in organic carbon and lithogenic fluxes in high altitude Pyrenean lakes, *Sci Rep*, 13,
1109 8586, <https://doi.org/10.1038/s41598-023-35233-1>, 2023.
- 1110 Vidaller, I., Revuelto, J., Izagirre, E., Rojas-Heredia, F., Alonso-González, E., Gascoin, S., René, P.,
1111 Berthier, E., Rico, I., Moreno, A., Serrano, E., Serreta, A., and López-Moreno, J. I.: Toward an
1112 Ice-Free Mountain Range: Demise of Pyrenean Glaciers During 2011–2020, *Geophys Res Lett*,
1113 48, <https://doi.org/10.1029/2021GL094339>, 2021.
- 1114 Welte, C., Wacker, L., Hattendorf, B., Christl, M., Koch, J., Synal, H.-A., and Günther, D.: Novel
1115 Laser Ablation Sampling Device for the Rapid Radiocarbon Analysis of Carbonate Samples by
1116 Accelerator Mass Spectrometry, *Radiocarbon*, 58, 419–435,
1117 <https://doi.org/10.1017/RDC.2016.6>, 2016.
- 1118 Zawiska, I., Luoto, T. P., Nevalainen, L., Tylmann, W., Jensen, T. C., Obremaska, M., Słowiński,
1119 M., Woszczyk, M., Schartau, A. K., and Walseng, B.: Climate variability and lake ecosystem
1120 responses in western Scandinavia (Norway) during the last Millennium, *Palaeogeography,
1121 Palaeoclimatology, Palaeoecology*, 466, 231–239,
1122 <https://doi.org/10.1016/j.palaeo.2016.11.034>, 2017.
- 1123

1124 **Figure captions**

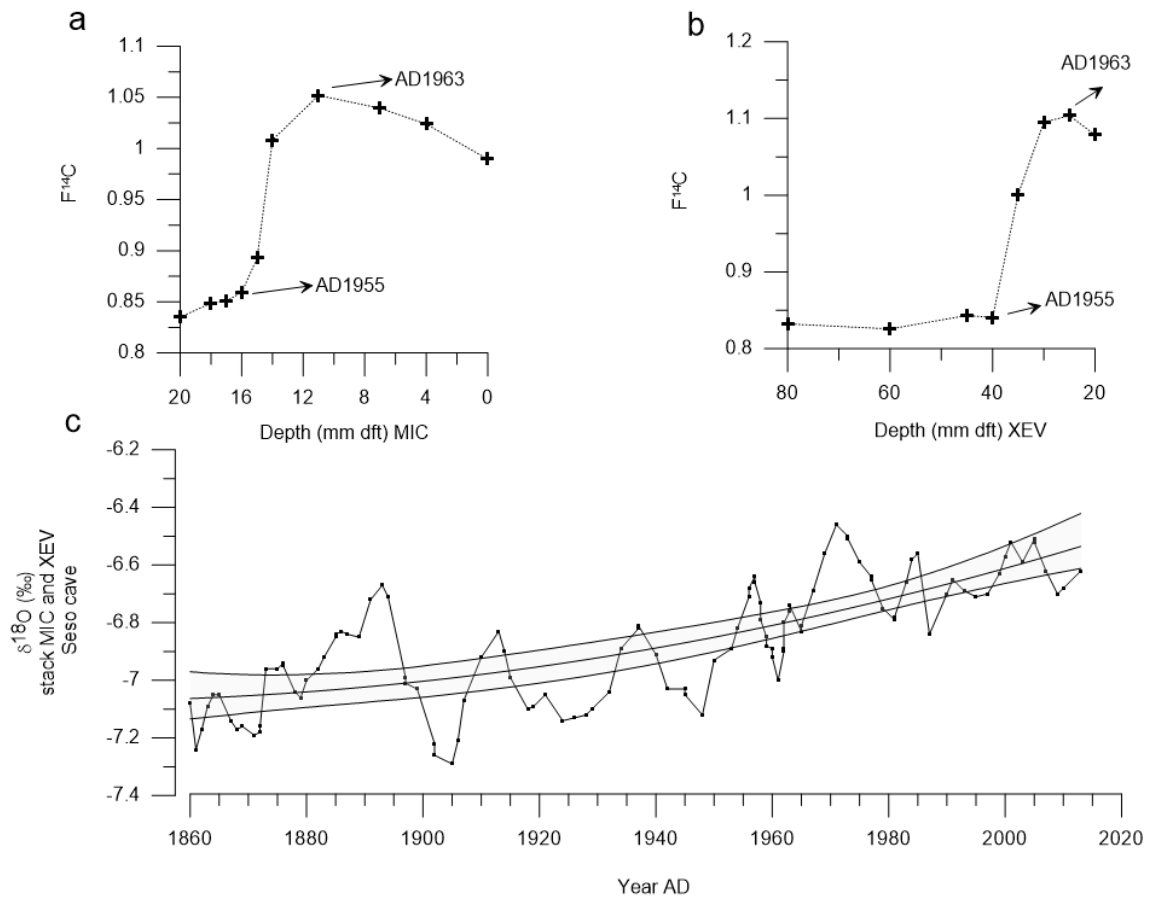
1125 **Figure 1.** a) Location of regional speleothem records covering last 2500 years to be compared with the
 1126 samples studied in the Pyrenees (red rectangle, enlarged in Fig. 1B). b) Location of caves (orange circles)
 1127 and other nearby records from northern Spain. See legend for the different types of available paleoclimate
 1128 archives. c) Location of the four studied caves in the Central Pyrenees of NE Spain in the vicinity of the
 1129 Ordesa and Monte Perdido National Park. Source base map: digital elevation model and hillshade derived
 1130 from Mapzen Global Terrain, coastline, boundaries and geographic lines from NaturalEarthData.com



1131

1132

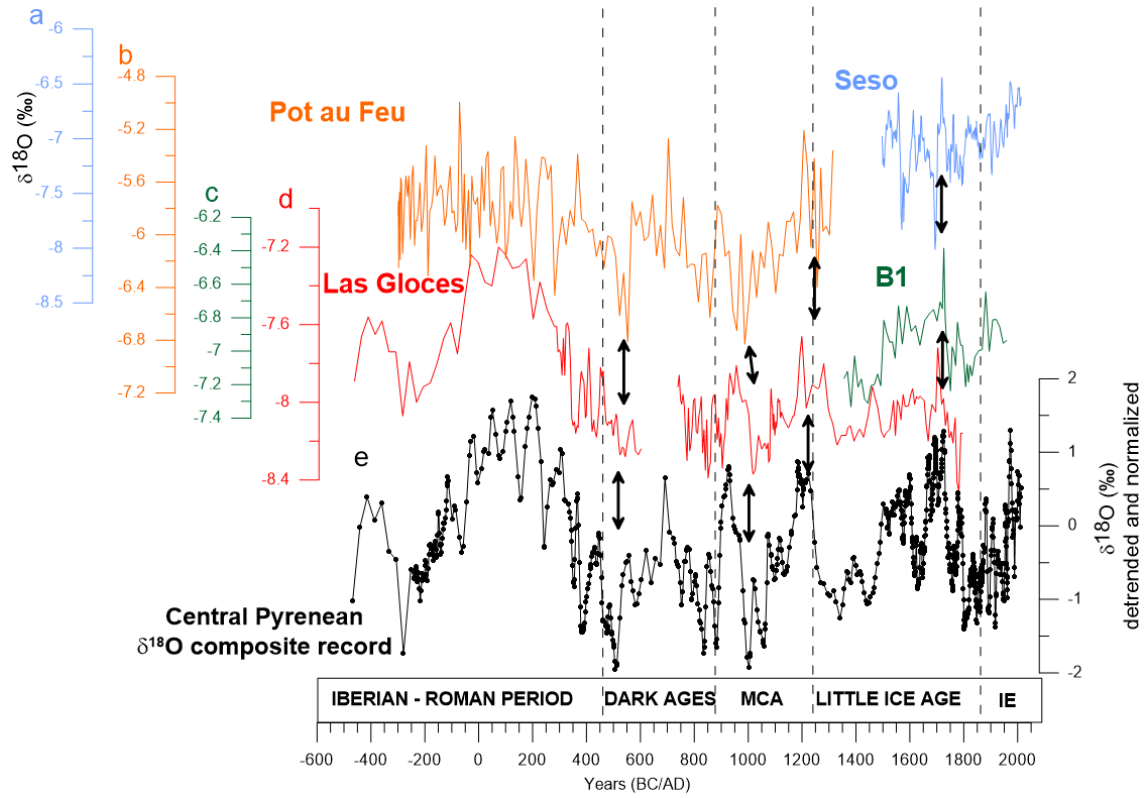
1133 **Figure 2.** ^{14}C activity (expressed as $F^{14}\text{C}$, following recommendations made in Reimer, 2004) of the top
 1134 parts of stalagmites MIC (a) and XEV (b) from Seso Cave. The start of the increase in $F^{14}\text{C}$ and its
 1135 maximum are recorded at 1955 and 1963 CE, respectively, in both stalagmites. c) Composite $\delta^{18}\text{O}$ record
 1136 using *Iscam* with data from MIC and XEV stalagmites.



1137

1138

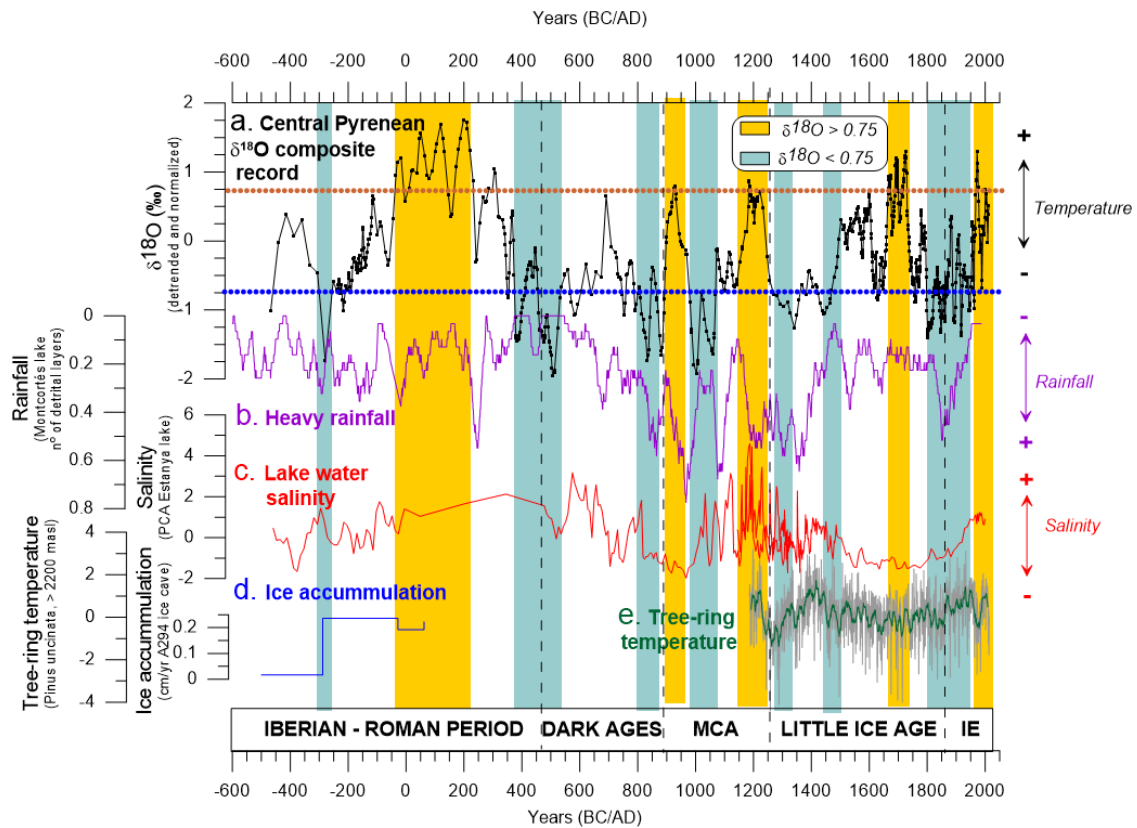
1139 **Figure 3.** Comparison of individual $\delta^{18}\text{O}$ records from four Pyrenean caves, (a) Seso; (b) Pot au Feu; (c)
 1140 B1 and (d) Las Gloces caves, and (e) the composite $\delta^{18}\text{O}$ record produced using *Iscam* (black curve) for the
 1141 last 2500 years. Generating Seso and Las Gloces curves required *Iscam* age modelling while Pot au Feu
 1142 and B1 curves represent only one stalagmite, which age model was produced by *StalAge* modelling. Black
 1143 double arrows indicate intervals with patterns present in all records. MCA: Medieval Climate Anomaly,
 1144 IE: Industrial Era.



1145

1146

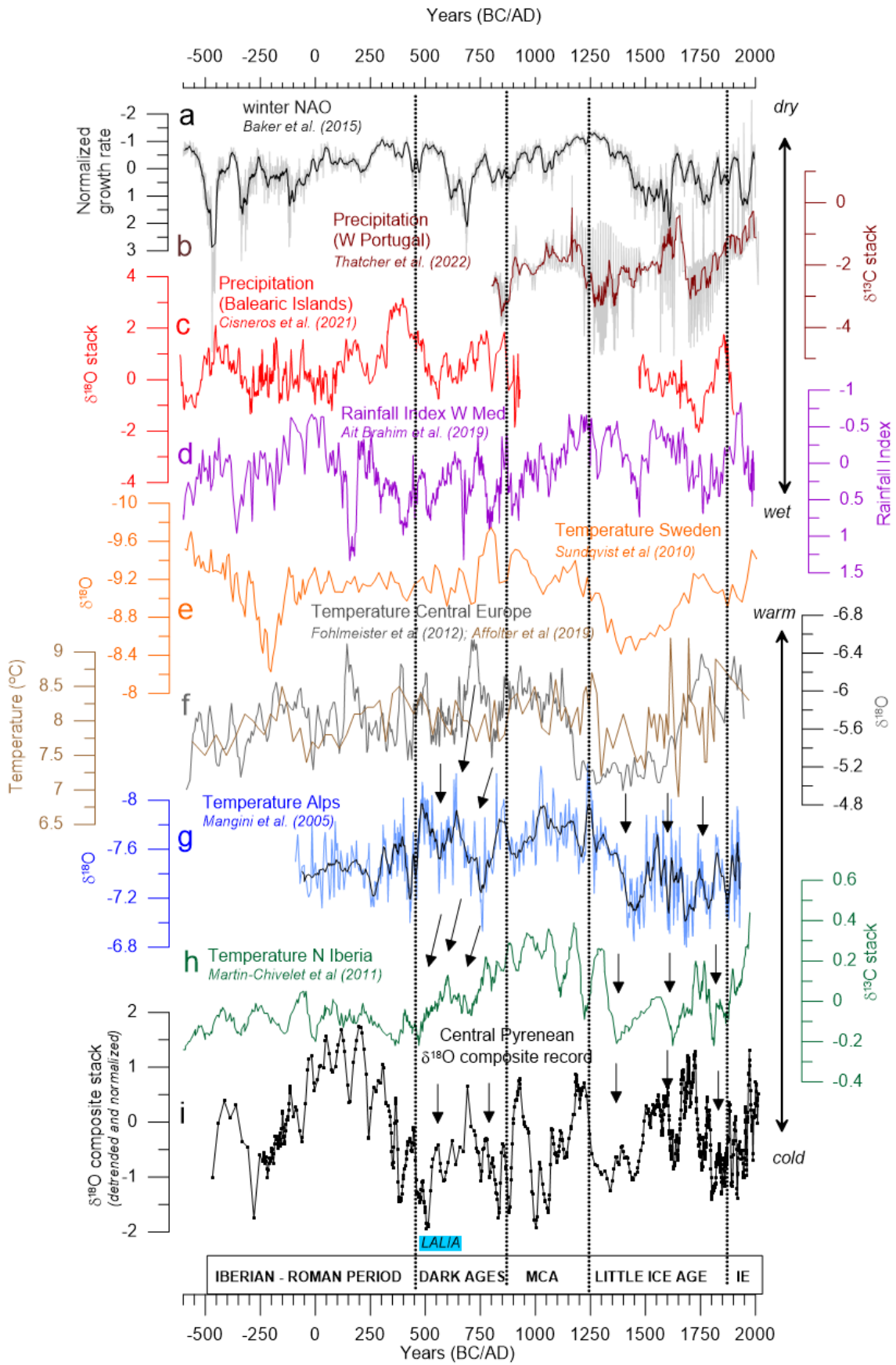
1147 **Figure 4.** a) Central Pyrenean $\delta^{18}\text{O}$ composite record for the last 2500 years based on eight stalagmites
 1148 from four caves. Blue bars mark intervals of $\delta^{18}\text{O}$ values below -0.75 , while yellow bars mark those with
 1149 $\delta^{18}\text{O}$ values above $+0.75$ (note this composite record was obtained from normalized records, so it varies
 1150 among -3 and 3 without possibility of direct translation to absolute $\delta^{18}\text{O}$ values). b) Rainfall reconstructed
 1151 from calcite layers from Montcortés lake in the Pre-Pyrenees (Corella et al., 2016). c) Salinity reconstructed
 1152 from geochemical data from Estanya lake in the Pre-Pyrenees (González-Sampéris et al., 2017; Morellón
 1153 et al., 2012, 2011). d) Snow and ice accumulation in ice cave A294 in the Cotiella massif of the Central
 1154 Pyrenees (Sancho et al., 2018), and e) Pyrenean temperature reconstruction based on tree-ring data
 1155 (Büntgen et al., 2017). MCA: Medieval Climate Anomaly, IE: Industrial Era.



1156

1157

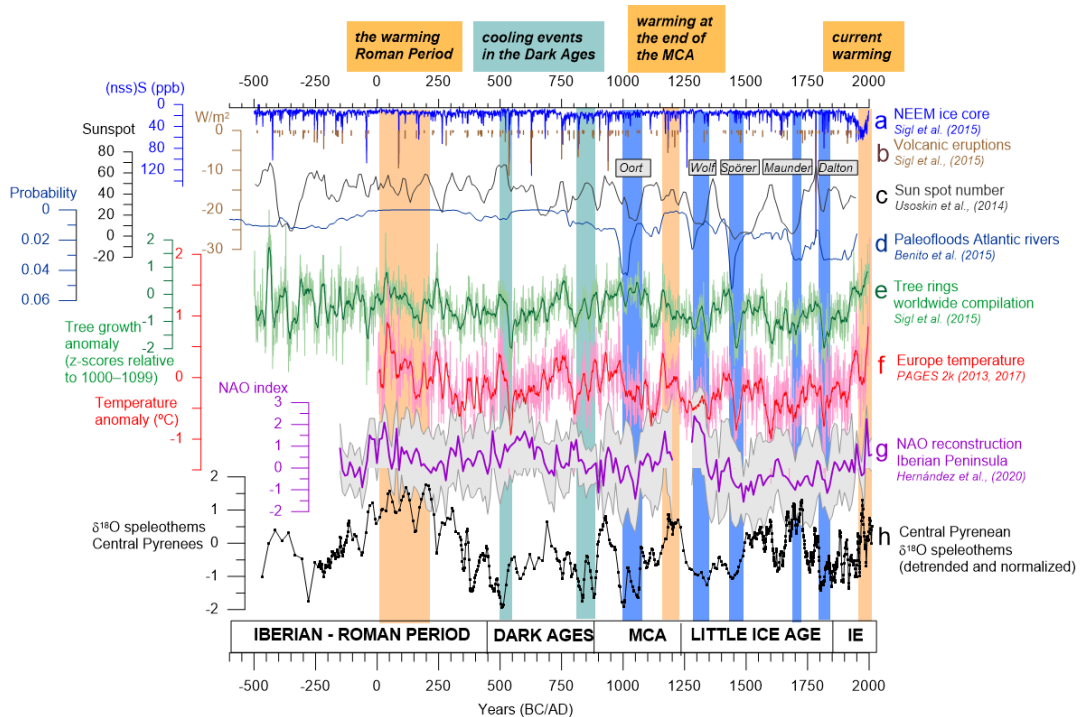
1158 **Figure 5.** Comparison of European and W Mediterranean speleothem records covering the last 2500 years.
1159 a) winter NAO reconstruction based on growth rate of Irish speleothems (Baker et al., 2015); b)
1160 precipitation variability reconstructed for W Portugal (Thatcher et al., 2022), c) Balearic Islands (Cisneros
1161 et al., 2021), and d) Morocco (Ait Brahim et al., 2019); temperature variation reconstructed from e) Sweden
1162 (Sundqvist et al., 2010), f) Central Europe (Affolter et al., 2019; Fohlmeister et al., 2012), g) Alps (Mangini
1163 et al., 2005) and h) Northern Iberia (Martín-Chivelet et al., 2011); i) Central Pyrenean $\delta^{18}\text{O}$ composite
1164 record (this study). Black arrows indicate intervals of well-reproduced patterns during the Dark Ages and
1165 the Little Ice Age cold intervals. MCA: Medieval Climate Anomaly, IE: Industrial Era.



1166

1167

1168 **Figure 6.** Global records and forcing mechanisms. a) volcanic forcing represented by the (nss)S (ppb) in
 1169 the NEEM ice core (blue line); b) changes in the irradiance as a consequence of Northern Hemisphere
 1170 volcanic eruptions (Sigl et al., 2015) (brown bars); c) sunspot numbers (Usoskin et al., 2014); d) probability
 1171 of paleofloods in European temperate regions (Benito et al., 2015); e) worldwide tree-ring compilation
 1172 (green line, running average width window = 15) (Sigl et al., 2015); f) temperature reconstruction from
 1173 Europe, compiled by the PAGES2k group (red line, running average width window = 15) (PAGES 2k
 1174 Consortium, 2013); g) the NAO reconstruction for the Central Iberian Peninsula (purple line) and the 95%
 1175 (light grey band) uncertainty intervals and h) Central Pyrenean $\delta^{18}\text{O}$ composite record (this study). Light
 1176 brown bars indicate warming periods during the Roman Period, the end of the MCA and in recent decades.
 1177 Light blue bands mark cooling events during the DA while dark blue bands mark solar minima (Oort, Wolf,
 1178 Spörer, Maunder and Dalton). MCA: Medieval Climate Anomaly, IE: Industrial Era.



1179

1180

1181 **Table 1.** Sample characteristics

Cave	Sample ID	Length (cm)	Number of U-Th dates (used in StalAge)	Interval covered (years BCE/CE in StalAge)	Sampling resolution (average years per isotope sample)	Comments
<i>Seso</i>	MIC	8.5	8	1718-2010 CE	3.8 years	Growth to present
	XEV	26	9	1501-2013 CE	1.9 years	Two growth periods, no hiatus. Growth to present
	CHA	8.5	3	1573-1779 CE	3.5 years	The uppermost 7 mm are not sampled
	CLA	10.5 (a hiatus at 8.5 cm)	4	1826-1935 CE	1.5 years	The uppermost 2 cm are not sampled
<i>Las Gloces</i>	ISA	13.5 (a hiatus at 7 cm)	7	346-607 CE 845-634 CE	11.4 years	In StalAge, one date is not included due to high error
	LUC	23.3 (a hiatus at 12.5 cm)	6	471BCE-504 CE 547-1991 CE	11.2 years	Really short hiatus
<i>B-1</i>	TAR	7.5 cm	8	1355-1959 CE	10.5 years	
<i>Pot au Feu</i>	JAR	80 cm	10	299BCE-1314 CE	10 years	

1182

1183

1184
1185
1186
1187
1188

Table 2. ²³⁰Th dating results of the eight stalagmites examined in this study (data from the University of Minnesota, University of Xi'an and University of Melbourne). Analytical errors are 2σ of the mean. The sample marked by a red asterisk was discarded due to the high error.

Sample ID	²³⁸ U (ppb)	²³² Th (ppb)	²³⁰ Th/ ²³² Th (t)	^g 230Th (measured)	^g 230Th/ ^g 232Th (a)	²³⁰ Th Age (yr) (uncorrected)	²³⁰ Th Age (yr) (corrected)	^g 230Th/ ^g 238U (corrected)	²³⁰ Th Age (yr BP) (corrected)
Sesio Cave									
Xer-0	451 ±1	12292 ±248	4.0 ±0.1	434.3 ±3.1	0.006 ±0.001	495 ±8	-52 ±87	454 ±3	115 ±387
Xer-5	335 ±1	2875 ±58	4.2 ±0.2	434.3 ±2.9	0.0021 ±0.0001	159 ±8	-6 ±116	434 ±3	-69 ±116
Xer-8	299 ±1	1557 ±31	8 ±0	424.6 ±3.1	0.0027 ±0.0001	204 ±9	97 ±76	425 ±3	34 ±76
Xer-110	308 ±1	798 ±16	18 ±1	410.5 ±2.4	0.0029 ±0.0001	223 ±9	170 ±39	411 ±2	107 ±39
Xer-145	267 ±1	535 ±11	25 ±1	404.7 ±2.7	0.0030 ±0.0001	256 ±10	195 ±31	405 ±3	132 ±31
Xer-190	261 ±1	340 ±7	54 ±2	419.0 ±2.8	0.0033 ±0.0001	328 ±10	301 ±22	419 ±3	238 ±22
Xer-210	299 ±1	1445 ±29	20 ±1	420.8 ±3.5	0.0039 ±0.0002	452 ±12	353 ±71	421 ±4	290 ±71
Xer-240	277 ±1	1758 ±35	19 ±1	436.4 ±2.7	0.0072 ±0.0002	548 ±12	420 ±92	437 ±3	357 ±92
Xer-280	339 ±1	2459 ±50	20 ±0	414.7 ±3.8	0.0086 ±0.0001	667 ±10	517 ±106	415 ±4	454 ±106
Mic-0	503 ±1	4623 ±93	5 ±0	485.9 ±2.4	0.0027 ±0.0001	196 ±6	16 ±128	486 ±2	-46 ±128
Mic-5	441 ±1	1166 ±23	6 ±1	487.3 ±2.3	0.0039 ±0.0002	69 ±11	17 ±38	487 ±2	-45 ±38
Mic-20	412 ±1	127 ±3	7.3 ±6	477.0 ±2.3	0.0014 ±0.0001	101 ±8	95 ±9	477 ±2	33 ±9
Mic-35	427 ±1	708 ±14	2.5 ±1	455.2 ±2.3	0.0025 ±0.0001	191 ±8	158 ±25	455 ±2	96 ±25
Mic-48	417 ±1	603 ±12	3.4 ±1	457.7 ±3.0	0.0030 ±0.0001	223 ±8	205 ±15	456 ±3	142 ±15
Mic-60	393 ±1	1049 ±21	2.3 ±1	461.4 ±3.8	0.0037 ±0.0001	274 ±8	242 ±24	462 ±4	179 ±24
Mic-67	413 ±1	3812 ±77	9 ±0	458.7 ±2.9	0.0051 ±0.0001	380 ±8	196 ±30	459 ±3	134 ±30
Mic-75	389 ±1	25715 ±517	4 ±0	458.0 ±2.5	0.014 ±0.0002	1080 ±15	267 ±576	458 ±3	204 ±576
Cha-0	346 ±1	332 ±7	3.4 ±2	371.5 ±3.1	0.0020 ±0.0001	158 ±9	138 ±17	372 ±3	75 ±17
Cha-25	368 ±1	493 ±10	3.2 ±1	367.1 ±2.9	0.0026 ±0.0001	204 ±8	176 ±22	367 ±3	113 ±22
Cha-70	346 ±1	1262 ±25	1.7 ±1	367.8 ±2.4	0.0030 ±0.0001	298 ±8	221 ±56	368 ±2	158 ±56
Cha-74	319 ±1	226 ±5	7.0 ±3	368.6 ±2.7	0.0030 ±0.0001	240 ±9	225 ±14	369 ±3	162 ±14
Cha-0	393.0 ±0.7	169 ±3	11.6 ±6	381.0 ±2.0	0.0030 ±0.0001	239 ±11	230 ±13	381 ±2	168 ±13
Cha-30	342.9 ±1.0	609 ±12	4.7 ±2	381.2 ±3.0	0.0030 ±0.0001	398 ±12	360 ±29	382 ±3	298 ±29
Cha-58	348.1 ±0.8	396 ±8	8.4 ±2	387.3 ±2.7	0.0038 ±0.0001	457 ±9	434 ±19	388 ±3	372 ±19
Las Glosas cave									
Isa-0	167.1 ±0.3	451 ±9	233 ±5	1465.3 ±3.4	0.0382 ±0.0003	1700 ±14	1668 ±26	1472 ±3	1605 ±26
Isa-4	119.9 ±0.2	291 ±6	221 ±5	1487.0 ±4.1	0.0325 ±0.0003	1454 ±15	1406 ±25	1493 ±3	1343 ±25
Isa-4.5	115.0 ±0.1	905 ±18	61 ±2	1510.8 ±1.9	0.0289 ±0.0004	1262 ±19	1171 ±67	1516 ±3	1108 ±67
Isa-6	107.7 ±0.2	832.2 ±171	5 ±1	1504.8 ±4.5	0.0253 ±0.0004	1107 ±20	185 ±63	1506 ±5	122 ±63
Isa-8	108.4 ±0.1	261 ±5	142 ±4	1504.6 ±3.6	0.0207 ±0.0004	905 ±17	877 ±26	1508 ±5	814 ±26
Isa-11	69.5 ±0.1	2977 ±60	8 ±1	1505.3 ±3.7	0.0201 ±0.0006	877 ±26	379 ±353	1507 ±4	316 ±353
Luc-0	113 ±1	2350 ±47	5.6 ±1	1859 ±4	0.0649 ±0.0006	2693 ±23	2483 ±150	1872 ±4	2420 ±150
Luc-5.5	88 ±1	539 ±11	12.7 ±3	1848 ±4	0.0649 ±0.0006	1806 ±18	1744 ±47	1857 ±4	1681 ±47
Luc-10	131 ±0.2	388 ±8	21.3 ±5	1721.6 ±3.2	0.0382 ±0.0003	1540 ±16	1508 ±27	1729 ±3.2	1445 ±27
Luc-11	81 ±1	955 ±19	50 ±1	1796 ±5	0.0359 ±0.0006	1407 ±23	1284 ±90	1803 ±5	1221 ±90
Luc-15.5	73 ±0	282 ±6	11.8 ±3	1783 ±6	0.0279 ±0.0006	1098 ±22	1057 ±36	1789 ±6	994 ±36
Luc-18.5	72 ±0	1477 ±30	1.6 ±1	1705 ±5	0.0202 ±0.0005	818 ±22	597 ±158	1708 ±5	534 ±158
Luc-22.5	139 ±0	287 ±6	4.7 ±2	1554 ±3	0.0058 ±0.0002	250 ±11	226 ±20	1555 ±3	163 ±20
Bl cave									
Bl-1.5-.56 mm	608 ±27	797 ±16	49 ±2	-288.5 ±2.5	0.00039 ±0.00002	59 ±3	54 ±5	-289 ±2	-9 ±5
Bl-1.5-.44 mm	6492 ±32	201 ±4	630 ±14	-295.8 ±1.8	0.00019 ±0.00001	184 ±2	182 ±2	-296 ±2	120 ±2
Bl-1.5-.37 mm	10036 ±47	616 ±12	392 ±9	-290.2 ±2.3	0.00146 ±0.00001	224 ±3	222 ±3	-290 ±2	159 ±3
Bl-1.5-.31 mm	8347 ±31	10930 ±219	2.0 ±1	-295.1 ±1.4	0.00019 ±0.00002	247 ±3	193 ±38	-295 ±1	130 ±38
Bl-1.5-.26 mm	7424 ±27	1633 ±33	15.6 ±3	-294.3 ±1.5	0.00208 ±0.00002	321 ±3	312 ±7	-295 ±2	249 ±7
Bl-1.5-.16 mm	8318 ±31	385 ±8	1052 ±33	-295.2 ±2.0	0.00295 ±0.00002	458 ±4	456 ±4	-296 ±2	393 ±4
Bl-1.5-.10 mm	9499 ±41	551 ±11	961 ±21	-290.9 ±1.5	0.00338 ±0.00002	521 ±4	519 ±4	-291 ±2	456 ±4
Bl-1.5-.0 mm	8128 ±33	649 ±13	884 ±18	-290.2 ±1.9	0.00428 ±0.00002	660 ±4	657 ±5	-291 ±2	594 ±5

U decay constants: $\lambda_{230} = 1.55125 \times 10^{-6}$ (Jaffey et al., 1971) and $\lambda_{234} = 2.82206 \times 10^{-6}$ (Cheng et al., 2013). Th decay constant: $\lambda_{230} = 9.1705 \times 10^{-6}$ (Cheng et al., 2013).

$g^{230}Th = ((^{234}U/^{238}U)_{activity} - 1) \times 10000$.

** $g^{230}Th_{initial}$ was calculated based on ^{230}Th age (T), i.e., $g^{230}Th_{initial} = g^{230}Th_{measured} \times e^{\lambda_{230}T}$.

Corrected ^{230}Th ages assume the initial $^{234}Th/^{238}U$ atomic ratio of $4.4 \pm 2.2 \times 10^{-6}$. Those are the values for a material at secular equilibrium, with the bulk earth $^{234}Th/^{238}U$ value of 3.8. The errors are arbitrarily assumed to be 50%.

***B.P. stands for "Before Present" where the "Present" is defined as the year 1950 A.D.

1189
1190

Pot au Feu cave										
Sample	^{238}U (ppb)	$^{230}\text{Th}/^{238}\text{U}$ (a)	$^{231}\text{U}/^{238}\text{U}$ (a)	$^{232}\text{Th}/^{238}\text{U}$ (a)	$^{230}\text{Th}/^{232}\text{Th}$ (a)	^{230}Th Age (yr) uncorrected	Age (yr BP) (b)	error	$^{234}\text{U}/^{238}\text{U}$ Initial (c)	
CT-PP 7.5	109	0.022	1.570	0.0084	2.6	1508	746	± 193	1.572	
CT-PP 47	NR	0.013	1.563	0.0017	7.3	884	733	± 79	1.565	
CT-PP 95	NR	0.014	1.580	0.0015	9.1	956	822	± 82	1.581	
CT-PP 205	95	0.019	1.565	0.0017	11.0	1330	1176	± 68	1.567	
CT-PP 335	NR	0.030	1.533	0.0051	5.8	2117	1652	± 253	1.536	
CT-PP 400	131	0.029	1.533	0.0033	8.6	2041	1739	± 140	1.535	
CT-PP 510	NR	0.033	1.534	0.0046	7.1	2347	1934	± 145	1.537	
CT-PP 640	103	0.036	1.600	0.0052	7.1	2503	2060	± 146	1.604	
CT-PP 740	109	0.022	1.570	0.0084	2.6	1508	2221	± 237	1.572	
CT-PP 790	NR	0.013	1.563	0.0017	7.3	884	2099	± 463	1.565	

(a) Activity ratios determined after Hellstrom (2003) using the decay constants of (Cheng et al., 2000)

(b) Age in kyr before present corrected for initial ^{230}Th using eqn. 1 of (Hellstrom, 2006) and $[\text{Th}/^{232}\text{Th}]$ of 0.9 ± 0.4

(c) Initial $[\text{Th}/^{238}\text{U}]$ calculated using corrected age

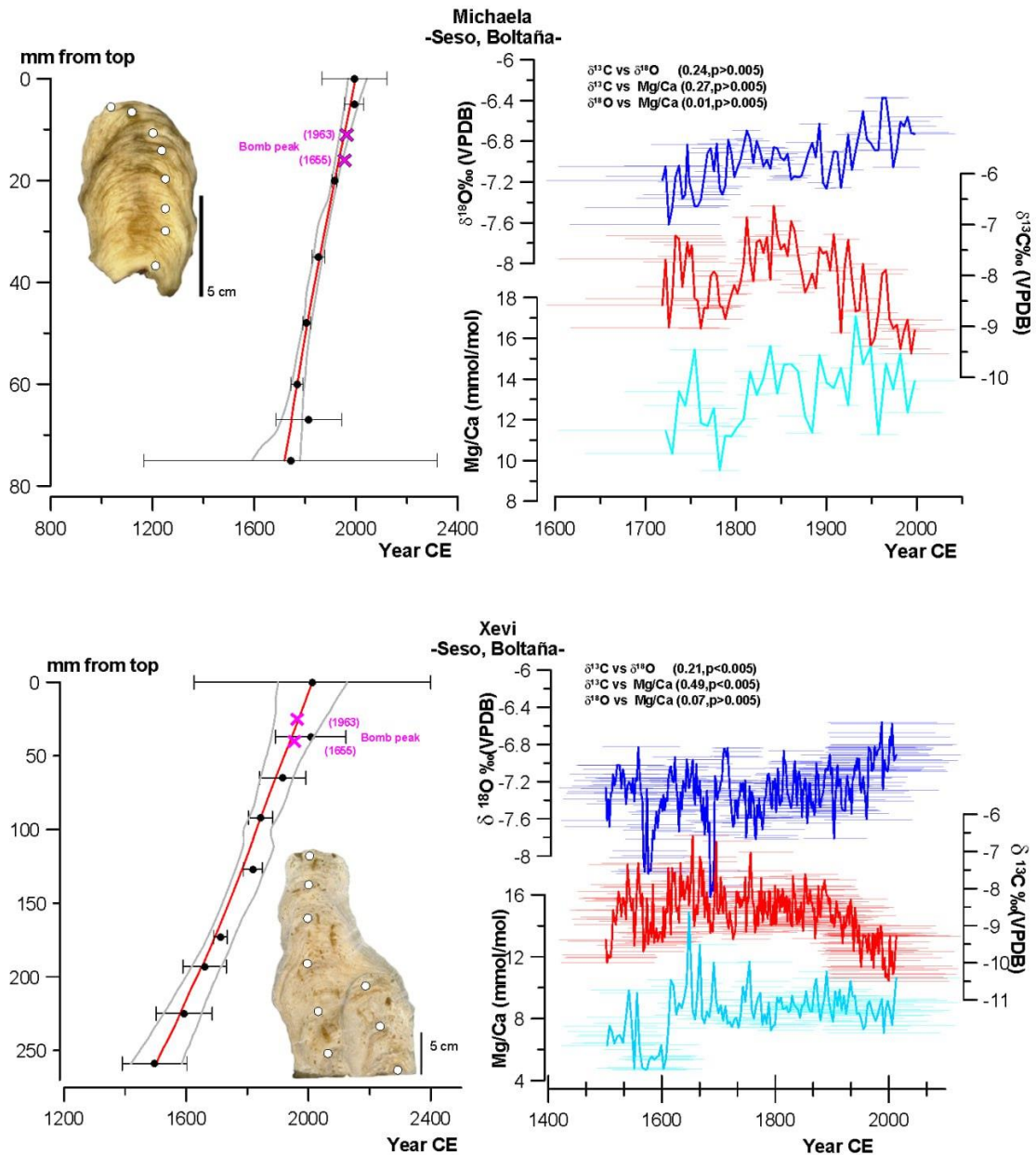
1191
1192
1193
1194

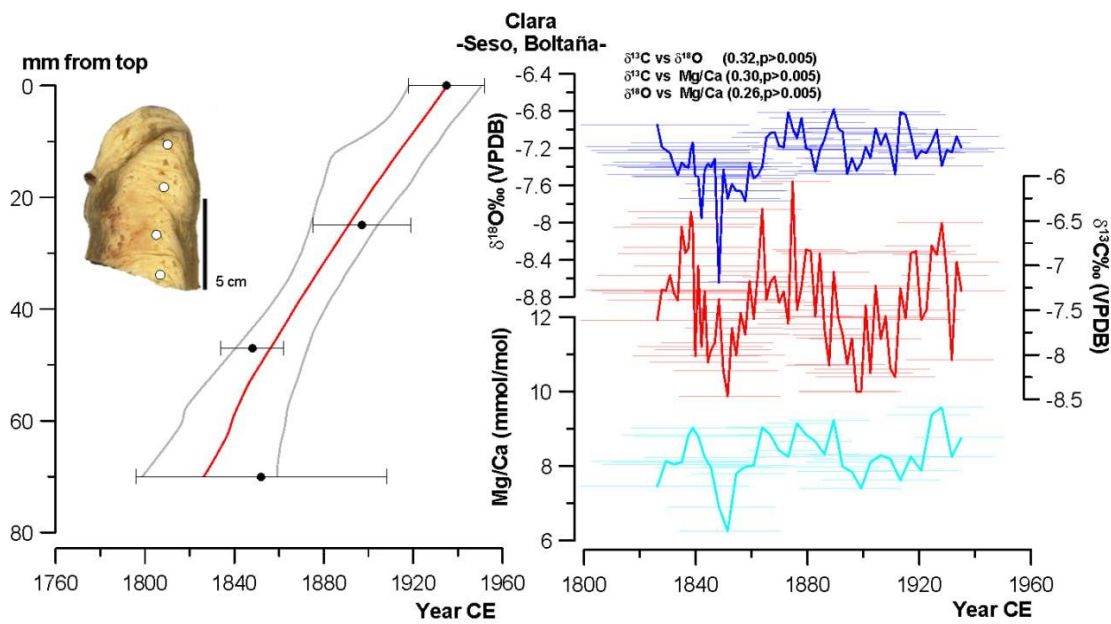
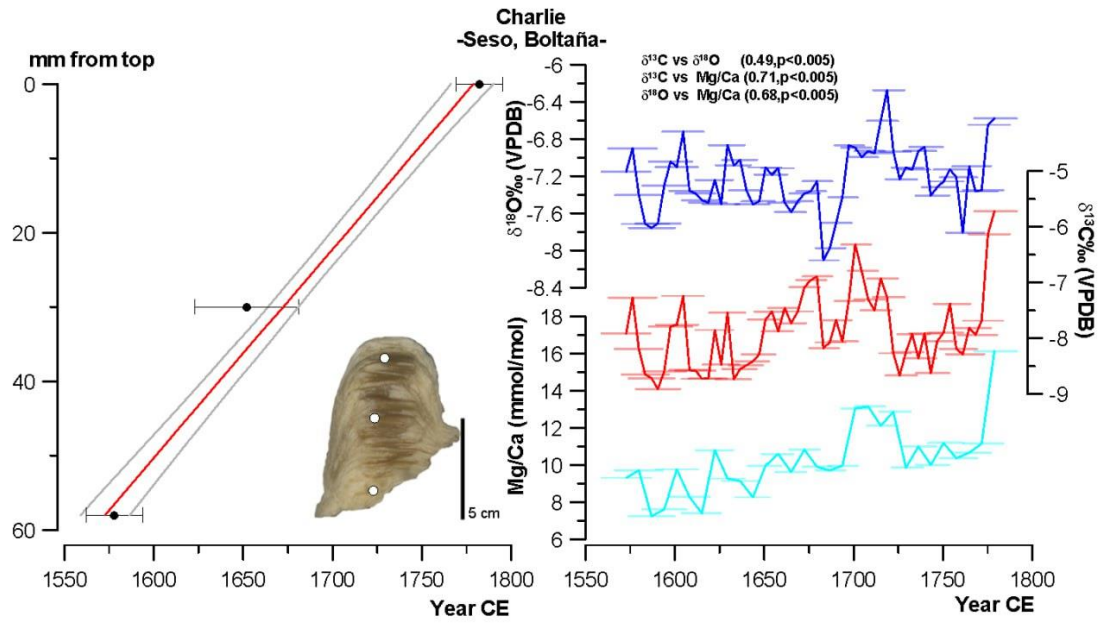
1195

1196 **Appendix A**

1197 **Figure A1.** Polished slabs, age-depth model using StalAge (left) and proxy profiles versus age (right) for the stalagmites used in this study arranged by cave (a. Seso, b. Las Gloces, c. B1, and d. Pot au Feu caves).
1198 the stalagmites used in this study arranged by cave (a. Seso, b. Las Gloces, c. B1, and d. Pot au Feu caves).
1199 Correlation coefficients among the three proxies are indicated based on Pearson correlation. Horizontal
1200 lines represent the age error for every data point, following StalAge uncertainty.

1201 a- Seso cave





1202

1203

1204

1205

1206

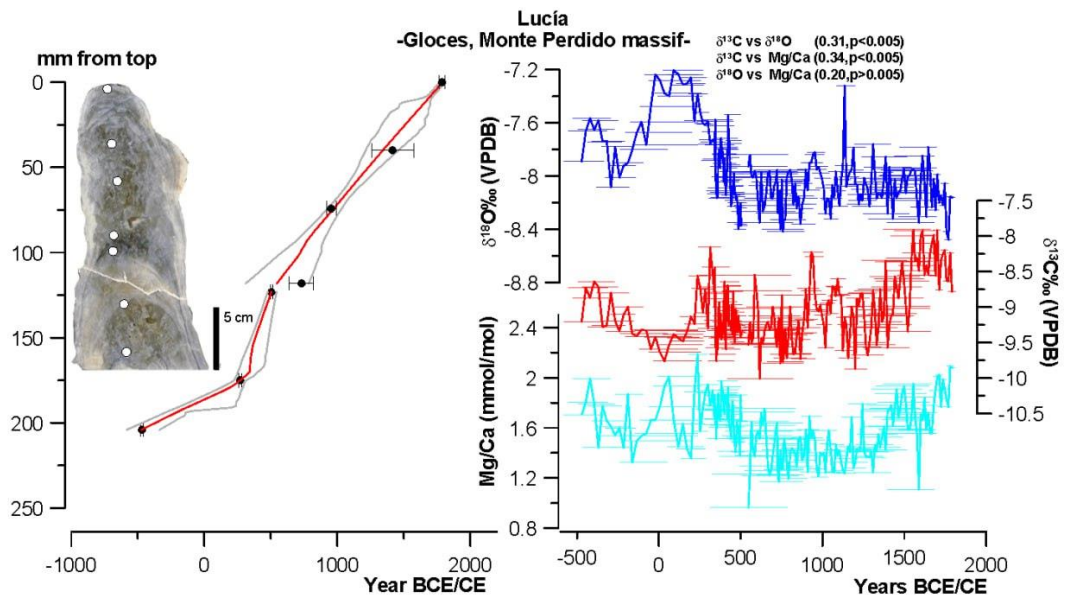
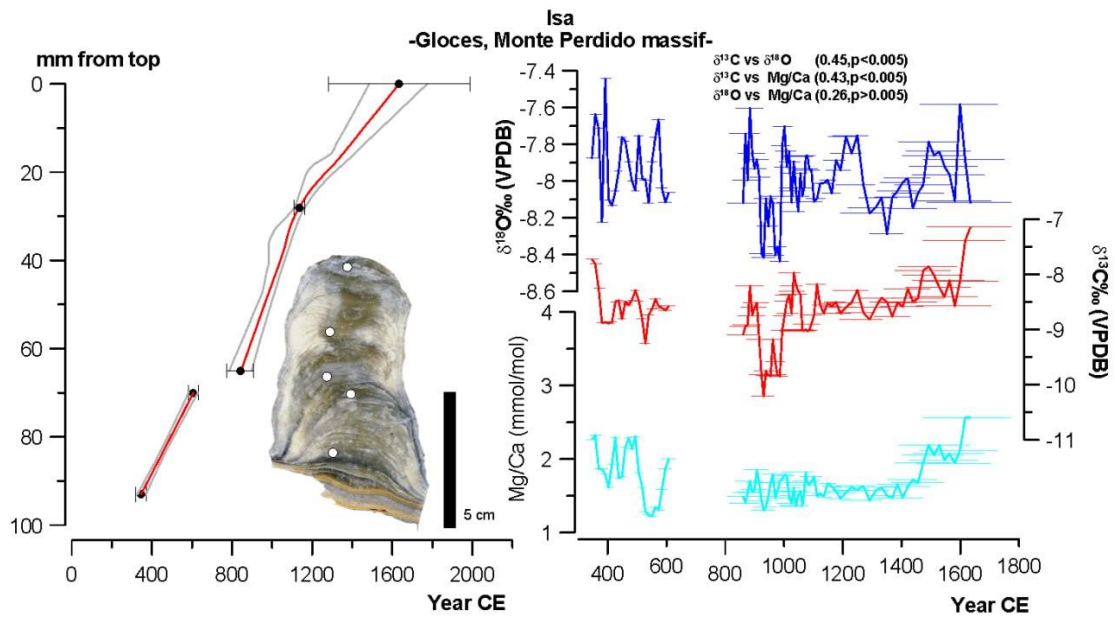
1207

1208

1209

1210

1211 b. Las Gloces cave



1212

1213

1214

1215

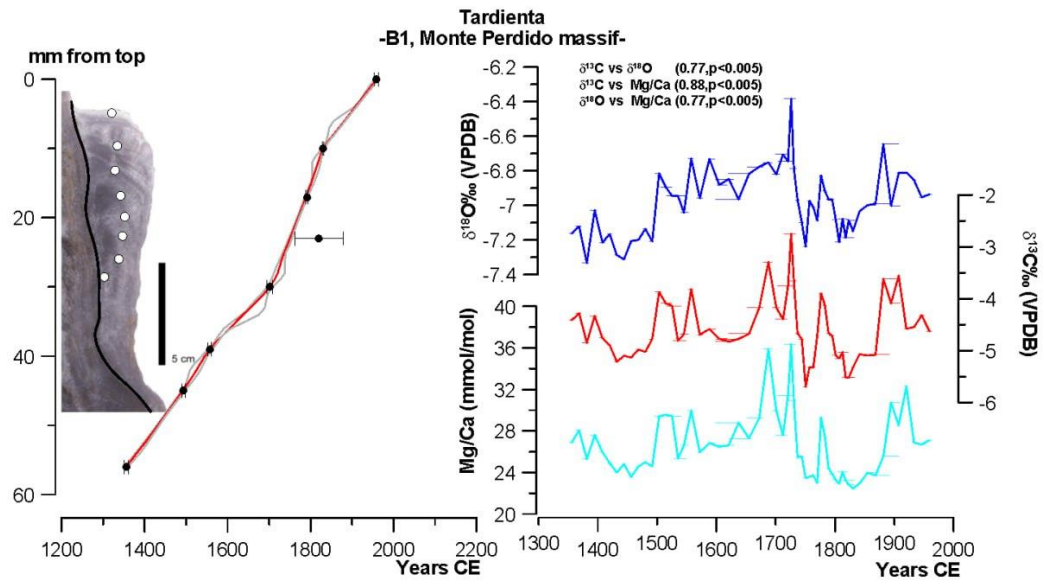
1216

1217

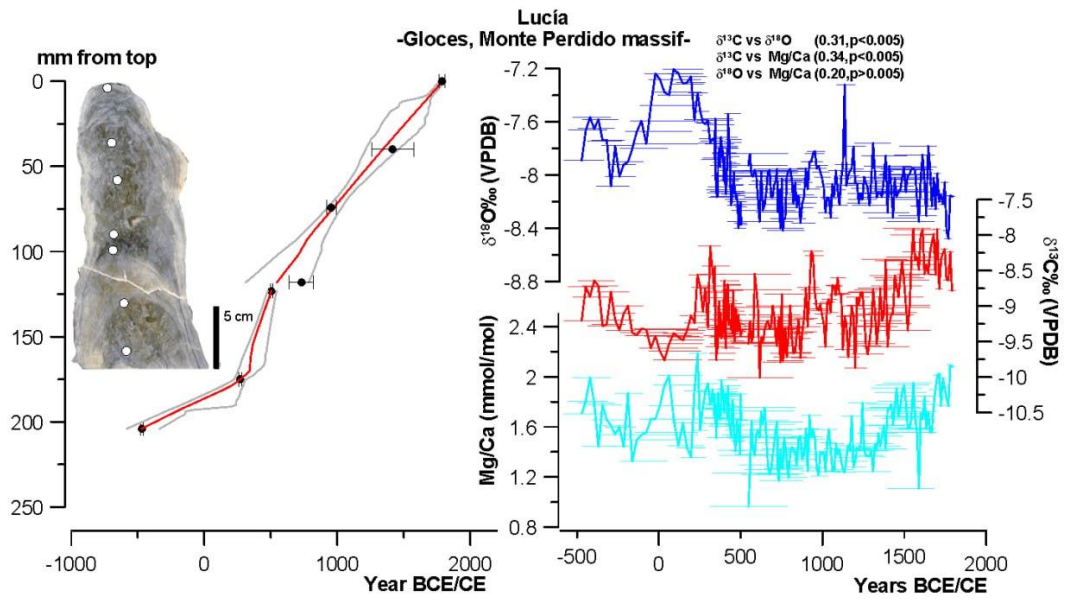
1218

1219

1220 c. B1 cave



1221 d. Pot au Feu cave



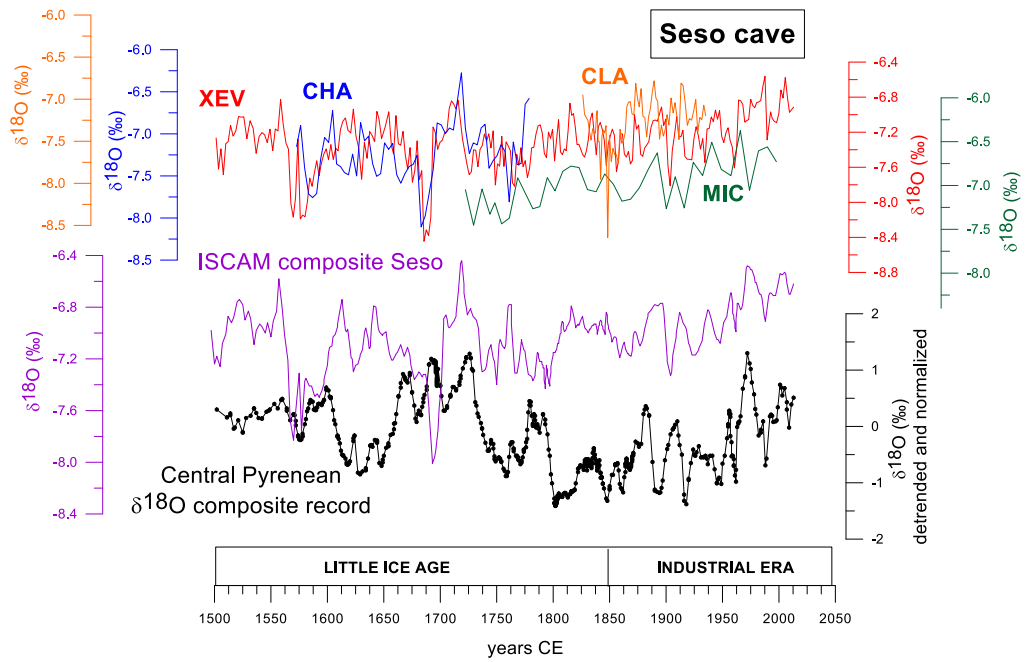
1222

1223

1224

1225 **Figure A2.** Construction of the composite $\delta^{18}\text{O}$ record for Seso cave. In the upper graph, the individual
1226 $\delta^{18}\text{O}$ profiles of the four Seso stalagmites are presented, using their StalAge models (XEV in red, CHA in
1227 blue, CLA in orange and MIC in green). Some records overlap (mostly between XEV and CHA and XEV
1228 and MIC). The composite $\delta^{18}\text{O}$ record for Seso cave is shown in purple on the same y-axis as the individual
1229 curves. The Central Pyrenees $\delta^{18}\text{O}$ composite record is shown at the bottom of the graph.

1230

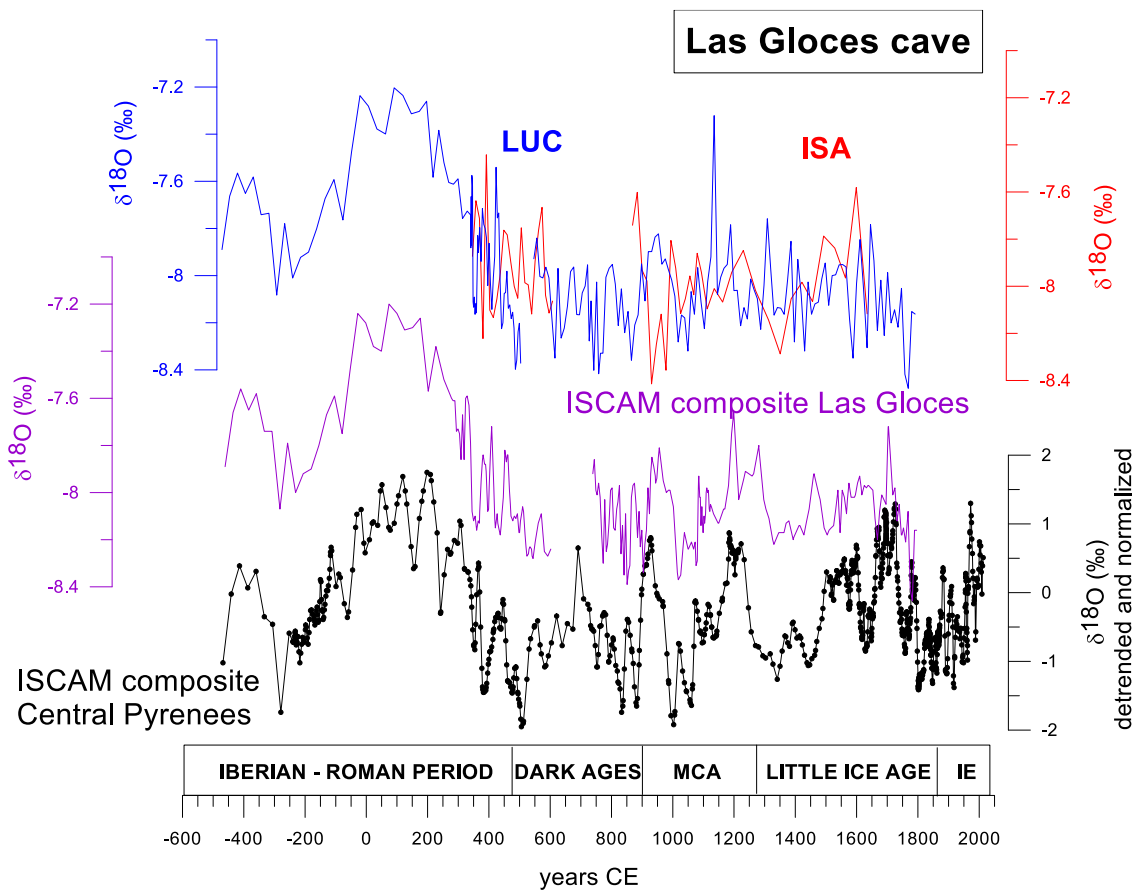


1231

1232

1233 **Figure A3.** Construction of the composite $\delta^{18}\text{O}$ record for Las Gloces cave. In the upper graph, the $\delta^{18}\text{O}$
1234 profiles of the two Las Gloces stalagmites are presented, using their StalAge models (ISA in red and LUC
1235 in blue). The composite $\delta^{18}\text{O}$ record for this cave is shown in purple curve on the same y-axis as the
1236 individual curves. The Central Pyrenees $\delta^{18}\text{O}$ composite record is shown at the bottom of the graph. MCA:
1237 Medieval Climate Anomaly, IE: Industrial Era.

1238

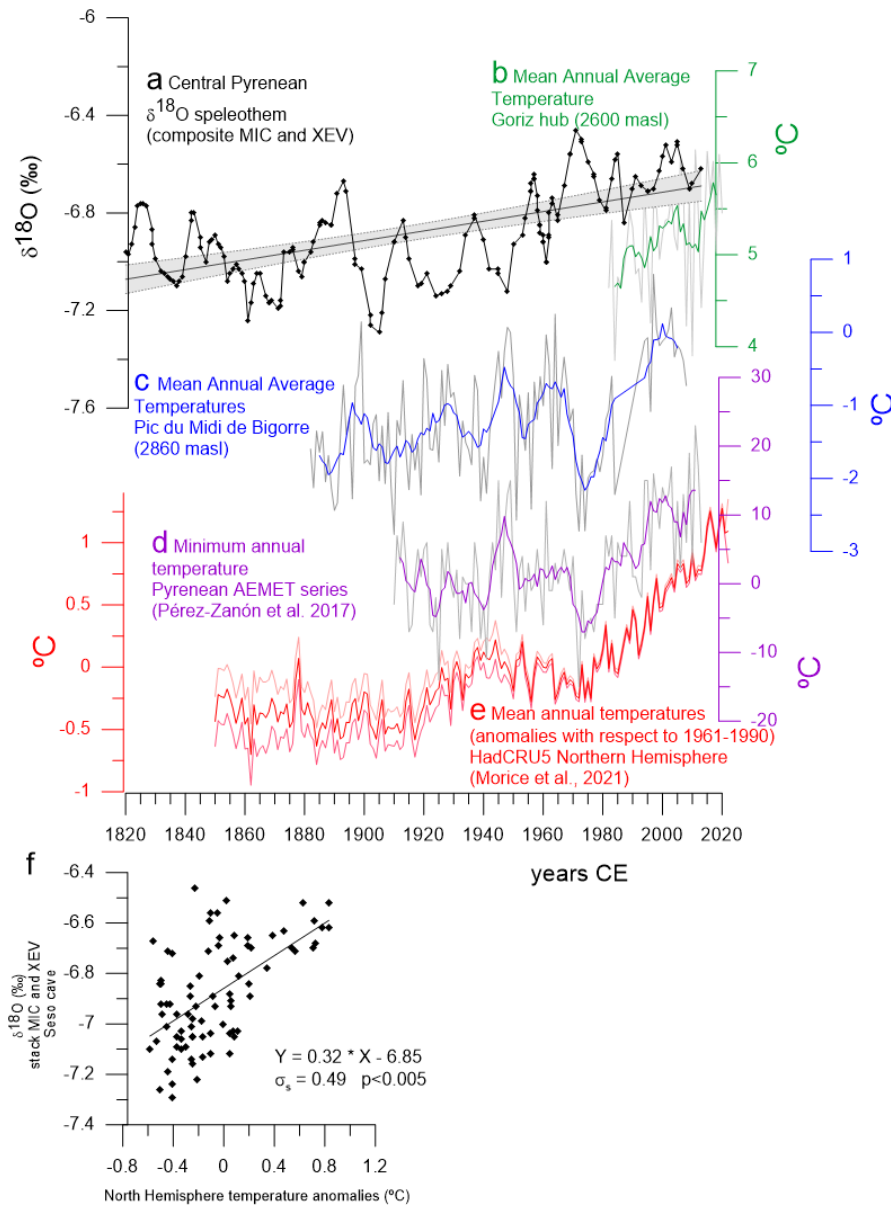


1239

1240

1241

1242 **Figure A4.** Correlation of (a) composite $\delta^{18}\text{O}$ record from MIC and XEV stalagmites with instrumental
 1243 temperature records at local, regional and global levels. (b) Mean Annual Average Temperature (MAAT)
 1244 from Goriz hub (AEMET data); (c) MAAT from Pic du Midi de Bigorre (Bücher and Dessens, 1991;
 1245 Dessens and Bücher, 1995); (d) Minimum Annual Temperature from the Pyrenees from AEMET series
 1246 (Pérez-Zanón et al., 2017) and (e) MAAT anomalies (respect to 1961-1990 years) using the HadCRUT
 1247 5.0.1.0. dataset (Morice et al., 2021). At the bottom, f) $\delta^{18}\text{O}$ values of the Pyrenees composite record (in a)
 1248 compared to North Hemisphere mean annual temperatures (in e) showing a significant correlation.



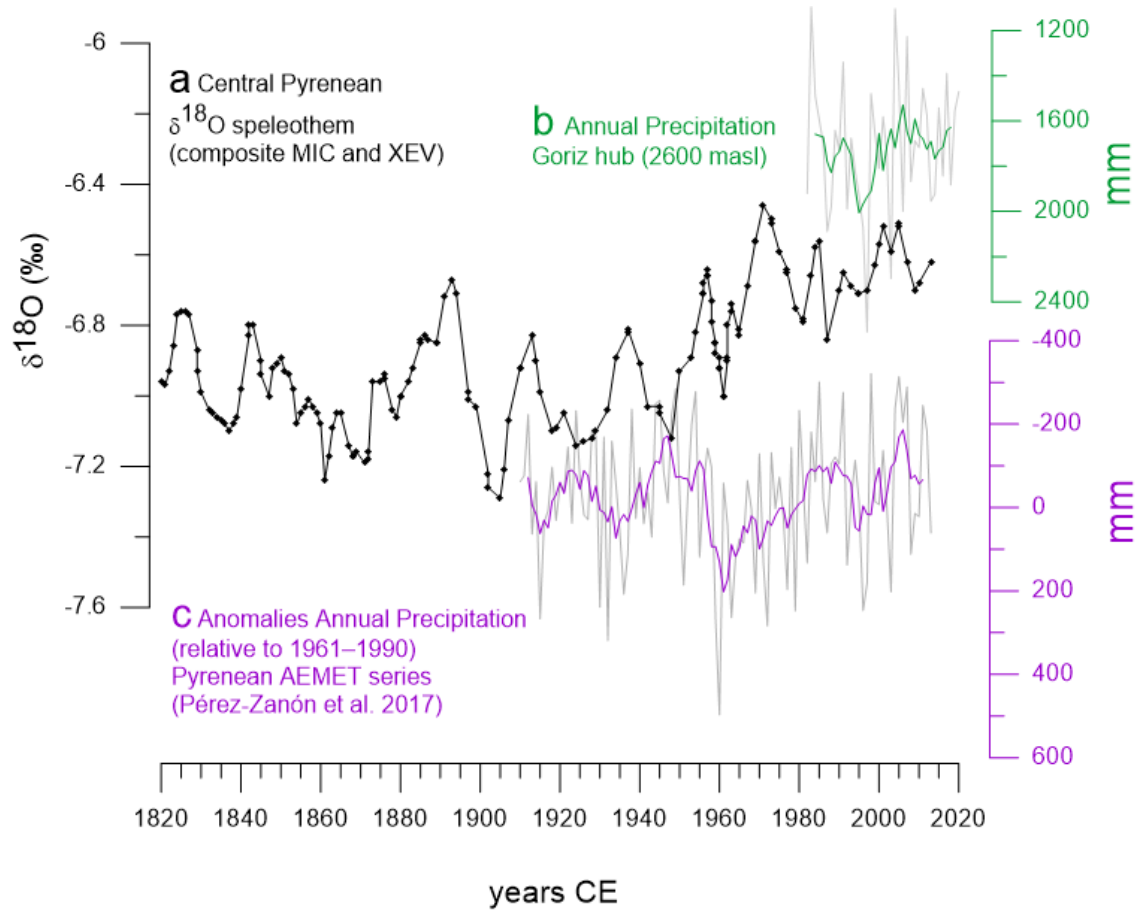
1249

1250

1251

1252 **Figure A5.** Correlation of (a) composite $\delta^{18}\text{O}$ record from MIC and XEV stalagmites with instrumental
1253 precipitation records at regional levels. (b) Annual precipitation from Goriz hub (AEMET data) and (c)
1254 Precipitation anomalies from the Pyrenees from AEMET series (respect to 1961-1990 years) (Bücher and
1255 Dessens, 1991; Dessens and Bücher, 1995). No significant correlation is observed.

1256



1257

1258